Planetary and Space Science 184 (2020) 104841

Contents lists available at ScienceDirect

Planetary and Space Science

journal homepage: www.elsevier.com/locate/pss

The Holy Grail: A road map for unlocking the climate record stored within Mars' polar layered deposits

Isaac B. Smith [a,b,*], Paul O. Hayne [c], Shane Byrne [d], Patricio Becerra [e], Melinda Kahre [f], Wendy Calvin [g], Christine Hvidberg [h], Sarah Milkovich [i], Peter Buhler [i], Margaret Landis [c], Briony Horgan [j], Armin Kleinböhl [i], Matthew R. Perry [b], Rachel Obbard [k], Jennifer Stern [l], Sylvain Piqueux [i], Nicolas Thomas [e], Kris Zacny [m], Lynn Carter [d], Lauren Edgar [n], Jeremy Emmett [o], Thomas Navarro [p,q], Jennifer Hanley [r], Michelle Koutnik [s], Nathaniel Putzig [b], Bryana L. Henderson [i], John W. Holt [d,i], Bethany Ehlmann [i,t], Sergio Parra [t], Daniel Lalich [u], Candice Hansen [v], Michael Hecht [w], Don Banfield [u], Ken Herkenhoff [n], David A. Paige [q], Mark Skidmore [x], Robert L. Staehle [i], Matthew Siegler [v]

[a] York University, Toronto, Ontario, M3J 1P3, Canada
[b] Planetary Science Institute, Lakewood, CO 80401, USA
[c] University of Colorado Boulder, Boulder, CO 80309, USA
[d] University of Arizona, Tucson, AZ 85721, USA
[e] Universität Bern, Bern, Switzerland
[f] NASA Ames Research Center, Moffett Field, California 94035, USA
[g] University of Nevada, Reno, NV 89557, USA
[h] University of Copenhagen, Copenhagen, Denmark
[i] Jet Propulsion Laboratory, California Institute of Technology, Pasadena, CA 91109, USA
[j] Purdue University, West Lafayette, IN 47907, USA
[k] SETI Institute, Mountain View, CA 94043, USA
[l] NASA Goddard Space Flight Center, Greenbelt, MD 20771, USA
[m] Honeybee Robotics, Pasadena, CA 91103, USA
[n] U.S. Geological Survey, Flagstaff, AZ 86001, USA
[o] New Mexico State University, Las Cruces, NM 88003, USA
[p] McGill Space Institute, McGill University, Montréal, Québec, Canada
[q] University of California, Los Angeles, CA 90095, USA
[r] Lowell Observatory, Flagstaff, AZ 86001, USA
[s] University of Washington, Seattle, WA 98195, USA
[t] California Institute of Technology, Pasadena, CA 91125, USA
[u] Cornell University, Ithaca, NY 14853, USA
[v] Planetary Science Institute, Tucson, AZ 85719, USA
[w] Haystack Observatory, Westford, MA 01886, USA
[x] Montana State University, Bozeman, MT 59717, USA

A B S T R A C T

In its polar layered deposits (PLD), Mars possesses a record of its recent climate, analogous to terrestrial ice sheets containing climate records on Earth. Each PLD is greater than 2 km thick and contains thousands of layers, each containing information on the climatic and atmospheric state during its deposition, creating a climate archive. With detailed measurements of layer composition, it may be possible to extract age, accumulation rates, atmospheric conditions, and surface activity at the time of deposition, among other important parameters; gaining the information would allow us to "read" the climate record. Because Mars has fewer complicating factors than Earth (e.g. oceans, biology, and human-modified climate), the planet offers a unique opportunity to study the history of a terrestrial planet's climate, which in turn can teach us about our own planet and the thousands of terrestrial exoplanets waiting to be discovered.

* Corresponding author. York University, Toronto, Ontario, M3J 1P3, Canada.
E-mail address: ibsmith@psi.edu (I.B. Smith).

https://doi.org/10.1016/j.pss.2020.104841
Received 1 May 2019; Received in revised form 26 December 2019; Accepted 9 January 2020
Available online 3 February 2020

During a two-part workshop, the Keck Institute for Space Studies (KISS) hosted 38 Mars scientists and engineers who focused on determining the measurements needed to extract the climate record contained in the PLD. The group converged on four fundamental questions that must be answered with the goal of interpreting the climate record and finding its history based on the climate drivers.

The group then proposed numerous measurements in order to answer these questions and detailed a sequence of missions and architecture to complete the measurements. In all, several missions are required, including an orbiter that can characterize the present climate and volatile reservoirs; a static reconnaissance lander capable of characterizing near surface atmospheric processes, annual accumulation, surface properties, and layer formation mechanism in the upper 50 cm of the PLD; a network of SmallSat landers focused on meteorology for ground truth of the low-altitude orbiter data; and finally, a second landed platform to access ~500 m of layers to measure layer variability through time. This mission architecture, with two landers, would meet the science goals and is designed to save costs compared to a single very capable landed mission. The rationale for this plan is presented below.

In this paper we discuss numerous aspects, including our motivation, background of polar science, the climate science that drives polar layer formation, modeling of the atmosphere and climate to create hypotheses for what the layers mean, and terrestrial analogs to climatological studies. Finally, we present a list of measurements and missions required to answer the four major questions and read the climate record.

1. What are present and past fluxes of volatiles, dust, and other materials into and out of the polar regions?
2. How do orbital forcing and exchange with other reservoirs affect those fluxes?
3. What chemical and physical processes form and modify layers?
4. What is the timespan, completeness, and temporal resolution of the climate history recorded in the PLD?

1. Background

1.1. Justification and timeliness

From a scientific point of view, this is the opportune time to set the direction of future exploration of the polar layered deposits (PLD). The Mars polar science community held a conference in 2016 (Smith et al., 2018) and the Mars Amazonian Climate Workshop in 2018 (Diniega and Smith, this issue) that distilled and summarized many years of research performed on the datasets of numerous missions. Further, the Mars Exploration Program Analysis Group (MEPAG) recently completed an ice and climate study identifying the polar regions as high priority destinations for future exploration (ICE-SAG, 2019). Those reports outline mature hypotheses and major themes for future work that cannot be addressed with current assets or those in development. Thus, we are at a turning point in the exploration of the PLD where existing data have been well-studied, hypotheses are waiting to be tested, and new data that can address these high priority topics are many years away.

Furthermore, technological developments have occurred in the past decade that make a landed polar mission more technically feasible and affordable than in the past. For example, entry, descent, and landing technology has evolved to include new methods of placing large payloads on the surface with greater location accuracy, and cryogenic drilling has advanced for both Mars and icy satellite investigations (Zacny and Bar-Cohen, 2010).

Much progress has been made in constructing theoretical models that relate different climate states to PLD accumulation and ablation (Levrard et al., 2007; Hvidberg et al., 2012; Manning et al., 2019). Several recent studies have compared Mars Reconnaissance Orbiter (MRO) observations of the layers to these models, and they show broad agreement on the recent accumulation rate of the northern PLD (NPLD, Becerra et al., 2016; Landis et al., 2016; Smith et al., 2016) and southern PLD (SPLD, Buhler et al., 2020). Thus, we, as a community, are ready to measure layer properties for the climate record they contain.

In that context, we present a mission architecture that takes advantage of all classes of NASA proposed mission programs. We focus on designing missions that could fit within the NASA Discovery, New Frontiers, and Small Innovative Missions for Planetary Exploration (SIMPLEX) programs i.e. programs that could develop significant payloads to reach Mars surface or orbit within the objectives of the Decadal Survey (National Research Council, 2011) Visions and Voyages (2013–2022) but not dominate the funding schedule. Therefore, we develop a campaign that begins with pathfinding exploration and orbital science that paves the way towards subsequent missions with a targeted set of questions to answer. The concepts are presented in Sections 2.C.1 through 2.C.4.

Ultimately, Mars polar exploration is of interest for many reasons. A primary interest is the climate record, but human exploration and the search for life may also lead us to the poles. Naturally, with the large quantities of surface ice exposed at the surface and 24+ hours of sunlight over long periods, polar ice could become a resource for human exploration. Likewise, the astrobiological potential of the layers may also be high. With abundant water, salts, and subsurface heating, a transient history of habitable environments may be recorded in the history of the polar caps. Therefore, while this paper focuses on the climate questions driving polar exploration, additional considerations should be included when selecting missions to the poles.

1.2. Mars Polar Science overview and state of the art

1.2.1. Polar ice deposits overview and present state of knowledge

The poles of Mars host approximately one million cubic kilometers of layered ice deposits (Smith et al., 2001, Fig. 1). Discovered by Mariner 9 imaging (Murray et al., 1972), these Polar Layered Deposits (PLD) have long been thought to record martian climate in an analogous way to terrestrial polar ice sheets. Both PLD are composed primarily of water ice (Plaut et al., 2007; Grima et al., 2009) but contain dust up to a few percent of their total mass, as well as materials potentially related to specific geologic events, such as volcanic ash and impact ejecta. The South PLD (SPLD) has an additional ~1% of carbon dioxide ice (CO_2) that resides in a stratified section above the H_2O layers (Phillips et al., 2011) and a thin, ~10 m thick, CO_2 residual cap that persists from year to year (Fig. 1). The vertical and horizontal distribution of these materials are thought to record atmospheric conditions including temperature, relative humidity, and aerosol dust content, along with atmospheric and isotopic materials that varied through time.

This iconic PLD layering is seen through visible and infrared imaging of bed exposures in troughs and scarps (Fig. 2) and radar sounding data (Fig. 3). Although the surfaces of the PLD are among the flattest and smoothest surfaces on Mars, they are bounded by steep, marginal scarps that typically expose up to a kilometer of vertical layering on slopes that exceed 10° and rarely reach 90°. Additionally, in the interior of the PLD, arcuate troughs expose a few hundred meters of bedding (Pathare and Paige, 2005). The marginal scarps appear to be erosional in nature, with active erosion observed at the steepest north polar examples (Russell et al., 2008). However, geologic structures, including unconformities, within the PLD indicate that the internal troughs are constructional features, and that they experience erosion on their steeper equator-facing walls and re-deposition on the pole-facing walls, leading them to have migrated 10s of kilometers poleward as the PLD accumulated (Howard et al., 1982; Howard, 2000; Smith and Holt, 2010, 2015; Smith et al., 2013).

Variations in the orbital configuration of Mars lead to climatic variations, which are thought to be recorded in the PLD. The orbital parameters, whose oscillations primarily drive these climatic changes, are the planet's obliquity, orbital eccentricity, and argument of perihelion (Laskar et al., 2002). Obliquity cycles have characteristic timescales of ~120 kyr and ~1 Myr; eccentricity varies on timescales of ~1.2 Myr; and the argument of perihelion has a precession cycle of ~51 kyr (Laskar et al., 2004). Over the last 20 Myrs, the obliquity of Mars has varied between 15 and 45°. High values of obliquity (>30°) mean that the horizontal surfaces on the poles receive more insolation on average than the mid-latitudes, which leads to the ablation of polar ice and transport to lower latitudes. Conversely, low obliquity promotes accumulation of polar ice. The present obliquity is around 25°, which is low enough that the average insolation at the poles is lower than at the mid-latitudes, but high enough that the net mass balance is difficult to distinguish from zero (Bapst et al., 2018). Obliquity variations between ~15 and ~35° straddle this value in the last 5 Ma and may have led to large variations in the rate of polar accumulation. Additionally, the precession of perihelion from southern summer (present state) to northern summer will affect insolation rates by 50% (Laskar et al., 2004). As with obliquity, this affects accumulation rates and therefore layer thickness.

Multiple angular unconformities in the stratigraphic record show periods of net ablation have occurred (Tanaka, 2005), and extremely dusty layers may be sublimation lag deposits that represent disconformities in the record (Fishbaugh et al., 2010). Orbital solutions also show that the mean obliquity between 5 and 20 Ma was ~35° – substantially higher than the ~25° from 4 Ma to the present. Unique solutions prior to 20 Ma cannot currently be derived, but statistical arguments show that a high mean obliquity is common and that the most probable obliquity over all of martian history is ~42° (Laskar et al., 2002). Thus, the current thick polar layered deposits may be atypical compared to most of martian history.

Impact craters on the uppermost surface of the NPLD yield a young age, implying ongoing resurfacing that is fast enough to erase craters 100 m in diameter over timescales of kyr to 10s of kyr (Banks et al., 2010; Landis et al., 2016). The SPLD crater record is consistent with a surface that is between 30 Ma and 100 Ma in age (Herkenhoff and Plaut, 2000; Koutnik et al., 2002). Model simulations of polar ice stability provide another age constraint. Several studies, described in sections below, argue that the high obliquities prior to 4–5 Ma make ice accumulation at the north pole impossible prior to that time. This has been interpreted as an upper limit for the age of the NPLD. However, the insulating effects of lag deposits are incompletely accounted for in these studies, and the obviously older SPLD and ice rich north polar basal unit (Tanaka, 2005) do not fit into this simple model. In addition, the SPLD (Becerra et al., 2019) and Basal Unit (Nerozzi and Holt, 2019) both most certainly contain climate signatures from their time of deposition.

In addition to the icy bedding that makes up most of their structure, the PLD are partly covered with bright residual ice caps that interact strongly with the current climate (Fig. 1). The north polar residual ice cap (NPRC) is a thin water ice unit that overlies the NPLD. It is exposed at the end of the spring after seasonal CO_2 and water frosts sublimate. Stereo imagery shows that it has less than a meter of relief and a texture of light and dark patches (or ridges in some locations) in repeating patterns with a horizontal scale on the order of decameters. It also exhibits an evolution of ice grain size and albedo throughout the year (Langevin et al., 2005; Brown et al., 2016). Fine-grained seasonal frost that accumulates in the fall and winter sublimates in the spring and summer, and older large-grained ice is exposed for a portion of the summer, suggesting that net ablation is currently occurring (Langevin et al., 2005). However, this large-grained ice is dust-free, and ablation has not been significant enough to produce a lag deposit, and ice is currently accumulating within polar impact craters (Landis et al., 2016).

The gross and net annual exchange of H_2O onto either polar cap is unknown, but the net flux is thought to average 0.5 kg m^{-2} over the last few Myr onto the NPLD. Evidence exists for either NPLD growth or loss in present day (Kieffer, 1990; Langevin et al., 2005; Chamberlain and Boynton, 2007; Brown et al., 2016) and for re-frosting during summer (Appéré et al., 2011), complicating the story. This unknown mass balance value is a critical parameter for even understanding the current climate, so knowledge of this value will help tune and validate GCMs of modern climate, which supports their application to understanding past climatic states.

The SPLD possess a partly buried reservoir of CO_2 ice (up to 1 km thick) that is comparable in mass to the current CO_2 atmosphere of the planet (Phillips et al., 2011; Bierson et al., 2016; Putzig et al., 2018). This CO_2 ice is capped by a water ice layer on top of which a much smaller (~1% of the current atmosphere) surface CO_2 South Polar Residual Cap (SPRC) ice deposit exists (Fig. 1; Bibring et al., 2005; Byrne and Ingersoll, 2003; Titus et al., 2003; Byrne, 2009). This deposit has extremely high albedo that changes with seasons (Colaprete et al., 2005; Schmidt et al., 2009) and hosts a wide variety of sublimation-driven erosional features that have been observed to grow and change every Mars year. Rapid changes in the morphology and appearance of the SPRC are evidence of its sensitive interaction with the current climate. Not only do these sublimation features grow by several meters per year (Thomas et al., 2009, 2016; Buhler et al., 2017), but summer dust storm activity has been observed to lead to distinctive bright halos on the edges of these features (Becerra et al., 2015), which may be associated with further wintertime condensation of CO_2 ice. This interaction, which we observe year to year,

Fig. 1. Images of the north and south polar layered deposits (NPLD and SPLD, respectively) from the High Resolution Stereo Camera on Mars Express. Left: NPLD in late spring without seasonal frost cover. Width of image is ~1250 km. Right: SPLD in late summer. White CO2 is the south polar residual cap (SPRC) and the youngest deposit visible at high latitudes and elevations. Much of the center of this image is water ice layers with a thick dust lag with similar coloration as the surrounding rocky surfaces. The NPLD also has a dust lag, but much of the white north polar residual cap (NPRC) is uncovered. The NPLD provides the majority of the water vapor budget for the planet.

may be direct evidence for new SPRC structures forming currently; however, they are very different from the water ice beds that comprise most of the SPLD volume.

1.2.2. Polar layered deposits formation and nature of layers

During orbital variations, the transfer of ice, aerosols, and dust from low latitudes to the poles causes the formation of alternating beds with variable ice purities. The bulk content of the NPLD is ~95% water ice (Grima et al., 2009). However, individual beds may be up to 50% dust (Lalich and Holt, 2017). The dust-rich beds may have formed during periods of high dust accumulation or during periods of ice loss and lag formation. Dust-poor beds must have formed during times when ice deposition was high relative to dust accumulation (Hvidberg et al., 2012). It is therefore necessary to study the visible stratigraphy of the PLD in order to interpret the timing of deposition of observed layers and build a climate record that ties bed sequences to particular insolation cycles in time.

1.2.2.1. Observing the stratigraphic record. Properties of the PLDs suggest that accumulation has not been uniform in space (horizontally) or time (vertically). Both PLDs are thickest near the pole and thinner at the margins; the thickest SPLD and south polar CO_2 deposits are slightly offset from the pole (Smith et al., 2001; Colaprete et al., 2005; Phillips et al., 2011; Putzig et al., 2018). In the NPLD, there are clear patterns of local and regional accumulation that were affected by existing basal topography (Brothers et al., 2015) or other large structures (e.g. a now buried chasma Holt et al. (2010)). Additionally, the PLDs contain numerous local and regional unconformities (Tanaka and Fortezzo, 2012) that are attributed to deposition following erosion by sublimation or wind ablation; however, some may have formed simultaneously (Smith et al., 2016).

The differences in relative accumulation with geographic location, unconformities, and post-depositional modification processes affect the final state of the sedimentary record in the PLD that we can observe. Therefore, in order to detect the periodic signals corresponding to the astronomically-forced insolation, we need to be able to observe and describe intrinsic properties of the beds that make up the record, i.e., properties that relate most closely to the environmental conditions at the time of accumulation. These properties may include sintering rate, dust/ice ratio, or concentrations of different isotopes in iced, dust, and trapped gases. On Earth, these properties can be extracted from ice or sediment core samples, but Mars conditions and remoteness make these measurements more difficult than on Earth. Once sampled, however, martian conditions may improve the readability of the layers over their terrestrial counterpart for several reasons.

1. Layers are conformable, particularly at depth, preserving them well compared to highly distorted ice seen in flowing ice on Earth.
2. The range of isotopic variation, particularly D/H is an order of magnitude greater than on Earth, making it easier to measure.
3. PLD ice's greater hardness due to lower temperature and Mars' lower gravity compared to Earth make drill holes much more stable against collapse (Bar-Cohen and Zacny, 2009).
4. The PLD likely lack firn (Paige et al., 1994; Arthern et al., 2000).

1.2.2.2. Remote sensing observations of exposed bed sequences. Orbital imaging at visible and infrared wavelengths has been used to extract information from the bedding outcrops exposed at the characteristic spiral troughs of the PLD (Cutts, 1973; Schenk and Moore, 2000). Visible imagery datasets provide information on brightness of layers, topography of the outcrop with stereo imaging (Becerra et al., 2016), and color-ratios, while infrared spectrometers provide estimates of the composition of ices, lithics, and alteration phases (e.g. Massé et al., 2012).

The High Resolution Imaging Science Experiment (HiRISE) (McEwen et al., 2007) on MRO, provides us with images from which we are able to extract reflectance and topographic information at the scale of ~1–2 m. There are noticeable variations with depth in topographic expression and brightness for every outcrop that point to an indirect relationship to the composition of the internal bedding (Becerra et al., 2016). Darker exposed layers are hypothesized to contain a higher dust content, and a more protruding layer may also be associated with a high dust content that insulates and protects that particular bed from erosion more than its stratigraphic neighbors (Malin and Edgett, 2001).

Surface observations are limited to the top 400–800 m of the PLDs, i.e., to the maximum depths of exposures. Additionally, the outcrops are scattered throughout the extent of the PLD, and therefore, correlations must be made between a sequence exposed in one location, and one exposed in a different one, which is not a trivial endeavor (Fishbaugh and Hvidberg, 2006; Milkovich and Plaut, 2008; Becerra et al., 2016).

The Compact Reconnaissance Imaging Spectrometer for Mars (CRISM; Murchie et al., 2007), also on MRO, provides visible/near-infrared spectra (VNIR; 0.3–2.6 μm) of the PLD at ~18 m/pixel resolution. This resolution cannot discern individual layers but can resolve broad trends and lag deposits. Lower spatial resolution (~300+ meter/pixel) VNIR spectra from the OMEGA imaging spectrometer onboard Mars Express (Bibring et al., 2005) have also been used to investigate the properties of the surface of the polar plateaus. These datasets have identified seasonal evolution in ice grain size (Langevin et al., 2005, 2007; Calvin et al., 2009, 2015; Brown et al., 2016) that can be observed for long periods (Piqueux et al., 2015), hydrated salts (possibly including perchlorate and sulfates) within the NPLD (Horgan et al., 2009; Massé et al., 2012), and the presence of primary mafic minerals within the NPLD (Sinha et al., 2019). Hydrated salts may reflect transient aqueous alteration on the polar surface (Horgan et al., 2009) and/or accumulation of atmospheric precipitates (Massé et al., 2012). Mafic minerals within the NPLD include pyroxene, olivine, and glass, both of sand size and finer, which are distinct from the homogeneous global dust that dominates the lag on many exposures. These layers are most likely sourced from a combination of distal and proximal impact

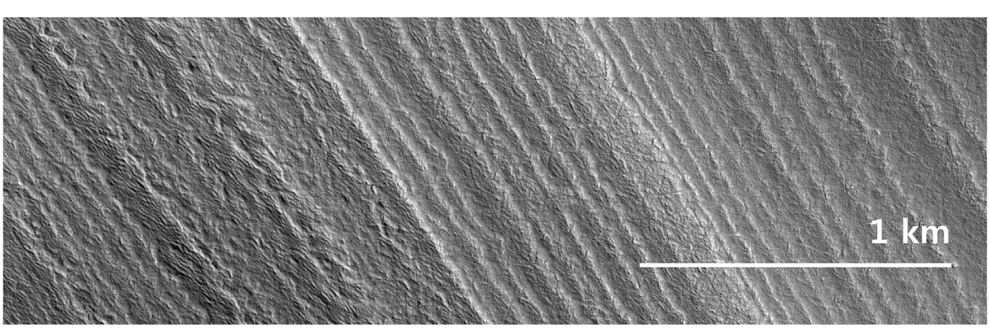

Fig. 2. HiRISE image PSP_005103_0995 of layers in the south polar layered deposits (SPLD). Exposed layers imply active and recent erosion; however, a dust lag may slow sublimation on annual time scales.

ejecta and distal volcanic ash (Horgan et al., 2014; Sinha et al., 2019). The north polar basal unit is also at least partially composed of similar mafic minerals, as the cavi unit is a major source of glass-rich sand feeding the north polar sand sea (Horgan and Bell, 2012).

1.2.2.3. Observations of the subsurface structure with radar. Radar instruments like the Mars Advanced Radar for Subsurface and Ionosphere Sounding (MARSIS (Picardi et al., 2004);) on board the European Space Agency's (ESA's) Mars Express, and the Shallow Radar (SHARAD (Seu et al., 2007);) on MRO, are sensitive to the dielectric properties of the target material. Ice is nearly transparent to radar waves, allowing the radio wave to penetrate to the deepest portions of the PLDs, as deep as 3.5 km, and permitting views of the internal structure (Figs. 3 and 4). These data show that the deposits are relatively pure, with up to 5–10% bulk dust concentrations for the NPLD and SPLD, respectively (Grima et al., 2009; Plaut et al., 2007). Recently, a very high reflection zone was detected at the bottom of the SPLD (Orosei et al., 2018); raising the possibility for a thin layer of water at the polar base.

Differences in silicic content (primarily dust, but possibly ash or ejecta) between icy layers will cause changes in dielectric permittivity that change the speed of propagation of the radar wave, causing a reflection (Nunes and Phillips, 2006). The relationship between permittivity, layer structure, and dust content is not completely understood. For example, radar signals from a series of thin, dust-rich beds may have similar properties to a single, thick dust-rich layer (Lalich and Holt, 2017). However complicated the layering may be, there is consensus that the radar response is related to the dust content of the PLD beds (Grima et al., 2009; Lalich and Holt, 2017).

The vertical resolution of current radar observations is much lower than that of optical imagery, causing a difficulty in matching visible layers and radar reflectors. Where comparisons have been made, radar reflectors mimic the exposed layers in spectral frequency and geometry, most likely because both types of observations observe variable concentrations of dust (Christian et al., 2013; Becerra et al., 2017a). Bed-to-bed correlation between datasets may not become possible until a higher resolution radar sounder flies to Mars in a polar orbit.

1.2.2.4. Large-scale geologic framework of the PLDs. Establishing broad-scale relationships between layer packets and geologic units in the PLDs provides the geologic framework within which the finer-scale stratigraphy must be analyzed and interpreted. In a major survey, Tanaka et al. (2007, 2008) searched for common characteristics and unconformities to develop a PLD-scale stratigraphic column and geologic map for both PLD. They derived the ages of the units from crater statistics and visual stratigraphic principles. The units most relevant to PLD stratigraphy are the formerly discussed SPRC and NPRC and multiple, thick water ice units (Tanaka et al., 2007, 2008; Tanaka and Fortezzo, 2012). The NPLD also reside over a km thick basal unit that contains ~50% sand (Fishbaugh and Head, 2005; Nerozzi and Holt, 2019).

1.2.2.5. Image-based correlation of exposed sequences. Studies of exposed layering rely on properties such as bed protrusion, local slope, and brightness that can be extracted from a Digital Terrain Model (DTM) or a single image of one location on the NPLD and compared to other locations. Images of bed exposures can be used to define and classify discrete layer sequences based on their morphological properties. From there, continuous depth profiles can be extracted and directly compared to synthetic stratigraphic columns built with models of ice and sediment accumulation.

Studies of the NPLD (Fishbaugh and Hvidberg, 2006) and of the SPLD (Byrne, 2004; Milkovich and Plaut, 2008; Milkovich et al., 2009) correlated spatially distinct sequences to propose the first relative stratigraphic columns for the two PLD. More recently, near complete imaging coverage of the PLD with the Context Imager (CTX) has allowed for individual beds to be traced hundreds of kilometers along the same trough (Becerra et al., 2016). These profiles can then be directly compared to climate proxies such as insolation or temperature changes with time (Laskar et al., 2002), or analyzed for periodic cycles that match those of the climate signals (Milkovich and Head, 2005; Herkenhoff et al., 2007; Perron and Huybers, 2009; Limaye et al., 2012; Becerra et al., 2017b).

1.2.2.6. Detailed stratigraphy of the NPLD. Fishbaugh et al. (2010b) were the first to construct a stratigraphic column based on topographic and morphologic considerations from a single HiRISE DTM. They defined two principal types of beds or bedding packets. These they called marker beds (MBs) after Malin and Edgett's (2001) identification of the "original" Marker Bed in various sites on the NPLD. Marker beds are thick, dark, have a characteristic hummocky texture, and thin, resistant layer sets each ~1–2 m in thickness. In the spacing between MBs, the authors reported finding the 30 m periodicity previously observed by Laskar et al. (2002) and Milkovich and Head (2005); and in the spacing between bedding packets (thin layers sets), they observed the 1.6 m wavelength from Perron and Huybers (2009). Later, Limaye et al. (2012) measured bed thicknesses from digital terrain models (DTMs) and found a low variance, with the majority of beds only few meters thick. Analysis by Limaye et al. (2012) confirmed the 1.6 m wavelength, but not the 30 m wavelength.

Recent work compiled a number of HiRISE DTMs to measure linear protrusion profiles and identified two dominant stratigraphic wavelengths in all profiles that have a common ratio of wavelengths of 1.98 ± 0.15 (Becerra et al., 2017a, 2017b). This was systematically lower than the 2.35 ratio of the orbital signals in the 2 Ma insolation (Laskar et al., 2002) but matches that of synthetic stratigraphy generated by the accumulation model of Hvidberg et al. (2012). These results appear to imply that the uppermost 500 m of the NPLD have accumulated at 0.54 mm/yr.

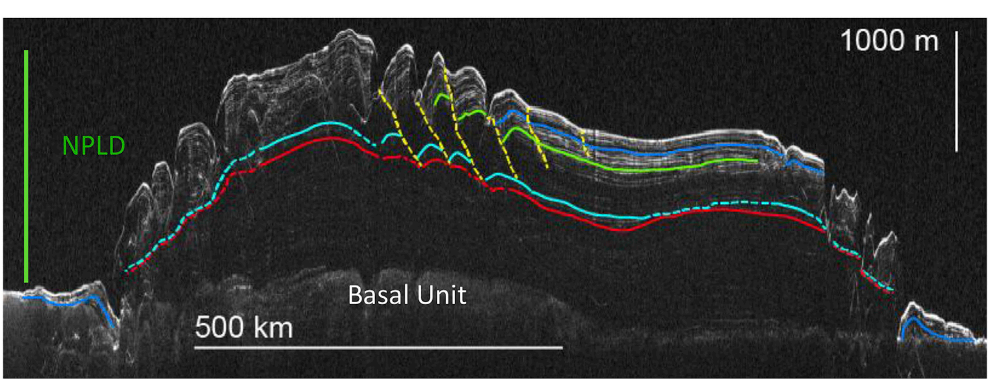

Fig. 3. Shallow radar (SHARAD) observation 1247002 exhibiting numerous reflections hinting at deposition cycles (Hvidberg et al., 2012). Annotation highlights mapped structures, including unconformities and discontinuities (yellow dashed lines). Modified from Smith and Holt (2015).

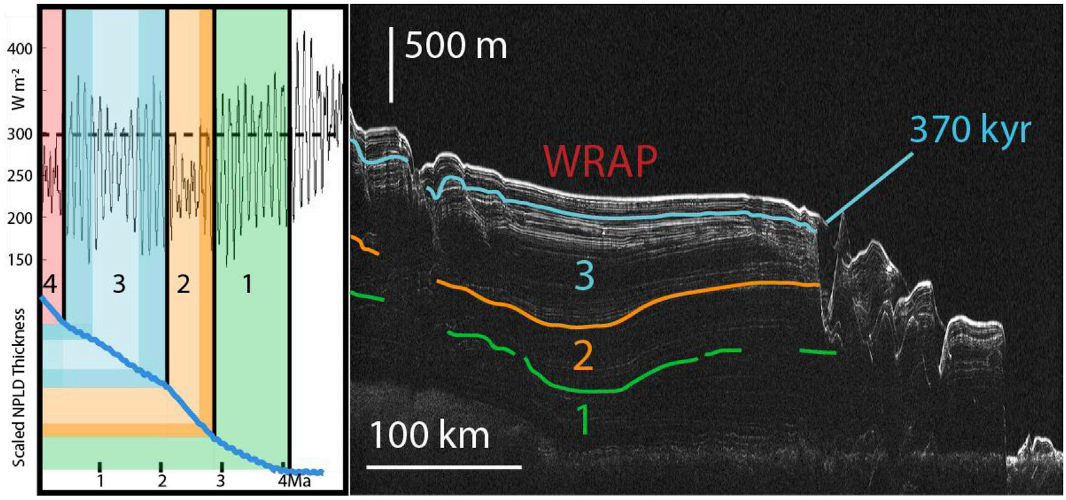

Fig. 4. Comparison of model from Levrard et al. (2007) (left) to radar stratigraphic mapping of the NPLD (right). Model calculates solar insolation in Wm-2 starting at ~4 Ma and predicts four distinct periods of NPLD accumulation, some at faster rates than others. Blue line in left panel is total accumulation of NPLD ice. Approximately 30 lag deposits are expected to derive from obliquity changes, similar in number to the total number of reflectors that SHARAD detects (right). Bright packets in the radar may correspond to periods when solar insolation cycles had larger amplitudes. WRAP is the Widespread Recent Accumulation Package, possibly associated with the current interglacial period (Smith et al., 2016). Adapted from Smith et al. (2016).

1.2.2.7. Radar-based stratigraphy. The ability to directly probe the vertical structure of the internal PLD, made possible by subsurface sounding radar, signified a substantial step forward in the study of Mars Polar Science (Figs. 3 and 4). One of the first major discoveries by SHARAD was that the NPLD beds are laterally continuous throughout almost the entire extent of the dome, over 1000 km (Phillips et al., 2008). When radar data coverage is dense enough, various radar units can be mapped throughout the whole PLD, resulting in thickness measurements of prominent units and, in essence, a radar-based stratigraphy (Putzig et al., 2009; Smith and Holt, 2015; Nerozzi and Holt, 2017). Additionally, a three-dimensional radar volume has been developed for observing in geometries not permitted with only two-dimensional, orbit parallel profiles (Foss et al., 2017; Putzig et al., 2018).

NPLD Reflections are location dependent, but radar images typically reveal ~ four packets of finely spaced bright reflectors separated by homogeneous interpacket regions and few reflectors (Fig. 4). Phillips et al. (2008) suggested that the packet/interpacket structure related to approximately million-year periodicities in Mars' obliquity and/or orbital eccentricity. Putzig et al. (2009) extended this work to suggest uniform deposition and erosion patterns were common throughout most of NPLD history. Studies with the SHARAD dataset also allowed researchers to explain the formation of Chasma Boreale (Holt et al., 2010) and the onset, migration, and morphological diversity of the iconic spiral troughs (Smith and Holt, 2010, 2015). Further, intermediate scale undulations reflect regional winds and leave behind stratigraphy that the radar detects (Herny et al., 2014). A full discussion of spiral trough formation hypotheses, including undulations, can be found in Smith et al. (2013).

Recent analysis of SHARAD data found a cap-wide unconformity that varied between 80 and 300 m beneath the current surface (Fig. 4, Smith et al., 2016). This was interpreted to represent a climatic shift from a period of net NPLD loss to one of rapid accumulation. Previous modeling had predicted thicknesses of ~300 m (Levrard et al., 2007) and volumes of approximately 1-m global equivalent layer of ice (Head et al., 2003) would have accumulated on the NPLD in the last 370 kyr. This thickness and volume compared favorably with the measured values, and Smith et al. (2016) interpreted this to mean that the unconformity occurred at this time and derived an average accumulation rate of 0.32 mm/yr since then.

1.2.2.8. Forcings. The climatic state of Mars is driven by changes in the orbital parameters of the planet and by the presence and longevity of volatile and dust reservoirs. As described above, obliquity variations are the most important orbital parameter driving the movement of water ice, potentially transferring the majority of Mars' water inventory between the mid-latitudes, poles, and equator on ~105 yr timescales (Levrard et al., 2007). Additionally, smaller effects on the pattern of global insolation occur due to precession of the argument of perihelion and variations in the eccentricity of Mars' orbit (Laskar et al., 2004). Combined, these three orbital cycles drive most of Mars' climate variations.

External forcings of Mars' climate include solar winds, Jeans Escape, cosmic rays, impactors, etc., that act to strip material away from the upper atmosphere or, on smaller scales, implant new materials. Secular mass loss driven by the solar wind put Mars into its current, low-pressure state billions of years ago (Jakosky and Phillips, 2001). On timescales relevant to the polar ice, atmospheric stripping may have affected fractionation rates for isotopes in parallel with solar cycles (Fisher, 2007).

There are also internal climate forcings. The major internal climate driver is the poorly understood dust cycle. Several local and regional dust storms occur repeatedly on annual time scales (Montabone et al., 2015). The biggest perturbation of the atmosphere by dust is from planet-encircling dust events that cover all longitudes and are so optically thick that visible imagers cannot detect the surface. In these events, atmospheric temperatures increase globally, affecting water vapor distribution and transport. Observations record dust storms every few martian years.

Volcanic outgassing must play a role in the variability of atmospheric composition and maybe pressure (Craddock and Greeley, 2009). The most recent volcanic eruptions are dated at only ~10 Myr, so they are relevant to Amazonian climate (Bermann and Hartmann, 2002). Evidence of eruptions, through fine grained pyroclastic ash fall or alteration of isotopic ratios into the atmosphere, may exist within the PLDs.

1.2.2.9. Isotope variability in layers. Because PLD layers form from meteoric constituents, they likely retain a combination of ices (H_2O, CO_2), dust, and trapped gasses. Water vapor and carbon dioxide will undergo fractionation processes during deposition to a solid, but trapped gases, if retained during sintering, can provide samples of the past atmosphere. Because of the numerous reservoirs that can contribute, the layers may be a collection of mixed sources.

The ratio of deuterium to hydrogen (D/H) in PLD water ice is a valuable measurement. The seasonal signal of D/H from atmosphere-ice exchange in the northern hemisphere imparts a distinctive isotopic signature in the atmosphere of >1000 per mil (Villanueva et al., 2015) that may be recorded in the currently forming ice layer. Over time, and through orbital cycles, the D/H ratio of layered ice will vary based on the source reservoirs that supply the materials (Vos et al., 2019). This deposition can tell us about the climate signal of orbital parameters driving variations in obliquity, which in turn provides information on what reservoirs are accessed at different orbital states (e.g., Montmessin et al., 2005; Fisher, 2007).

Even though multiple sources likely supplied the atmospheric water vapor that contributed to deposition in the PLDs, finding the ratio of D/H within solid ice will provide insight into the long-term (>3 Ga) climate history of Mars (Vos et al., 2019). This in turn will teach us about the loss rate of water to space (Jakosky, 2012) and Mars' earlier environment.

A key aspect of interpreting the PLD climatic record is establishing an absolute chronology in addition to relative timing. As with Curiosity (Farley et al., 2014), *in situ* geochronology with mass spectroscopy may be possible for the ice cores, particular for those layers enriched in dust. Methods measuring decay products of radioactive elements (e.g. He, Ne, Be, Ar) and the concentrations of cosmogenic radionuclides need further study to vet their application for the chronology of PLD (Section 2.A.5).

1.2.2.10. Polar ice flow. Terrestrial ice sheets experience rapid, large-scale flow that affects layer properties, including thickness, slope, and stratigraphic continuity. These post-deposition modifications alter the climatological record, complicating our efforts to interpret it. If the PLD of Mars have undergone measurable flow, then we must be prepared to take this into account when choosing sampling locations and interpreting the Martian climate record.

The magnitude of flow at the NPLD is debated. Predictions of large-scale flow at the NPLD have been made for decades (e.g. Fisher, 1993, 2000; Fisher et al., 2010; Winebrenner et al., 2008; Sori et al.,. 2016), but observational investigations directly testing these hypotheses with stratigraphic comparisons do not support predictions of widescale flow (Karlsson et al., 2011; Smith and Holt, 2015), even though some forms of predicted flow may not result in evidence of stratigraphic thinning or thickening (Fisher et al., 2010). Additionally, the thickness of layers in the lowermost 1 km should vary with distance from the accumulation to ablation zones or vary based on elevation gradients; however, they are essentially constant across the entire cap within the resolution of radar sounding investigations (Phillips et al., 2008; Putzig et al., 2009; Nerozzi and Holt, 2017).

In this paper we acknowledge the importance of flow in terrestrial ice sheets and their potential importance at Mars. Therefore, each recommended investigation below should be taken in context of the state of knowledge regarding flow.

1.2.2.10.1. Layer formation. Modern processes related to layer formation are not well known, and yet the current surface will one day become incorporated into the PLD, analogous to layers below. Thus, reading the variability in layer composition through time requires an understanding of what goes into making a layer today. Importantly, layer formation doesn't end upon burial. Like on Earth, there is a zone in which communication with the atmosphere still occurs, cosmic radiation interacts with materials, and internal forces can recrystallize the ice and exclude or incorporate impurities. Because of this, determining all of the processes that are recorded in a layer is a critical step towards reading the sequence of layers for a climate record.

Formation of a layer within the PLD begins with the accumulation and densification of atmospheric ice as snow into firn or by direct deposition that eventually fills pores by compaction, sintering, and gas diffusion. The ratio of these types of accumulation is unknown, but models of PLD accumulation and thermal inertia measurements suggest that the surface layer is dense, implying that densification may be rapid and the firn only a few cm thick (Arthern et al., 2000).

Observations by the near-polar Phoenix lander showed accumulation by both water ice crystals and surface frosts (Whiteway et al., 2009), but the accumulation ratios there were not quantified. Some of the water ice may also fall as nucleation centers in CO_2 ice, which comes seasonally and forms a meter-thick layer before subliming in the spring, potentially leaving the water ice and other constituents for incorporation into the uppermost layer (Colaprete et al., 2008; Brown et al., 2014).

Surface ice crystals begin small but grow with time. Terrestrial models and observation of this growth process show that it is limited by impurities (e.g. Durand, 2006; Barr and Milkovich, 2008). Past models of the martian PLDs (Kieffer, 1990) can relate ice grain size to depth in the upper meters to surface accumulation rate. These effects must be integrated through time to the depth at which atmospheric communication is cut off and metamorphosis ceases. Thus, measuring a buried layer without knowing what forms and modifies a layer will provide less information than if we have context on all of the formation mechanisms.

Besides meteoric ice, the PLD are expected to contain many other constituents. In decreasing order by volume, we expect the composition to include dust, salts, lithic materials, gas bubbles, and HDO, an isotopologue of H_2O, and daughter products of nuclear fission. Dust is incorporated either by falling out of the sky or scavenging during snow formation. Salts are also likely meteorically deposited or are brought in from winds that cross the pole. Depending on location, some of these materials may be recycled from older PLD layers that erode or sublime and are then transported to another place for incorporation. Lithic material, such as volcanic ash or impact ejecta probably fall irregularly. Bubbles of atmospheric gas likely form as new ice accumulates above. Additionally, cosmic radiation will bombard the uppermost PLD, triggering reactions that leave measurable products that vary with depth.

Investigating layer formation is critical to reading the climate record, because layers comprise the record. Many processes occur exactly at the surface, including ice crystallization, dust entrainment, isotope fractionation, heat loss or gain, and grain growth. Furthermore, processes continue even after burial, such a sintering, phase partitioning, and impurity exclusion. A firn layer permits gas exchange with the atmosphere, so the top centimeters may be actively forming. Prior work has found conflicting lines of evidence about the current mass balance of the NPLD (Kieffer, 1990; Langevin et al., 2005; Chamberlain and Boynton, 2007; Brown et al., 2016), so it is unclear even if the NPLD is currently gaining or losing mass.

1.2.3. Reservoirs other than the PLDs

It is important to identify the reservoirs of volatiles that can be mobilized. The atmosphere is the most active reservoir, and other reservoirs of dust and water ice are abundant on the planet. Each provides input to the climate state and PLD growth.

Carbon dioxide is the primary constituent of the martian atmosphere, with a mass of $\sim 2.5 \times 10^{16}$ kg (James and North, 1982). This fluctuates by approximately 1/3 each season as the atmosphere freezes to the winter pole (Tillman et al., 1993; Forget and Pollack, 1996). The SPRC contains additional CO_2 mass (<1% the mass of the atmosphere; Thomas et al., 2016). The other major reservoir of CO_2 ice is buried beneath the surface of the SPLD. The volume of this ice is estimated to be as much as 16,500 km^3 (Putzig et al., 2018) and if released to the atmosphere would more than double the surface pressure everywhere. This unit has sequences of deposition (Bierson et al., 2016), suggestive of climate signals (Manning et al., 2019; Buhler et al., in press) going back as far as many 10^5 years. Smaller CO_2 reservoirs exist that may play important roles in climate: regolith, minerals, and potentially clathrates.

Water ice is the volatile in greatest quantity on the planet, outweighing CO_2 by many orders of magnitude. Combined, the PLDs contain more than 2/3 of the known water budget of Mars (Levy et al., 2014). Additionally, mid-latitude glaciers and ice sheets make up another large fraction of the water budget (Levy et al., 2014; Karlsson et al., 2015). Smaller known reservoirs include water bound in the regolith to minerals or salts, in the atmosphere as clouds, and pore filling ice. Water may also be injected into the atmosphere via volcanoes or comets. Deep water reservoirs are predicted to exist, but they may not interact with the surface of the planet in a measurable way (Grimm et al., 2017).

Finally, dust reservoirs are found across much of the planet. The PLD may contain upwards of 5% dust for the north or 10% for the south based on dielectric (Plaut et al., 2007; Grima et al., 2009) and gravity (Zuber et al., 2007) measurements. Other locations on the planet, such as pedestal craters, contain stratified ice and dust as well (Kadish et al., 2008; Nunes et al., 2011). Atmospheric dust is visible from ground-based imagery, and many locations on Mars have a fine layer of surface dust.

Forcings, as discussed above, act on the volatile and dust reservoirs. However, there is abundant evidence that some of these reservoirs are much older than their expected response time to orbital variations (Levrard et al., 2007; Bramson et al., 2017 and references within). The presence of the SPLD is the biggest enigma because, unlike the NPLD, the surface age is an order of magnitude older than climate models would suggest (Herkenhoff and Plaut, 2000; Levrard et al., 2007). Also, mid-latitude ice shows crater counts that suggest ages of 10^8 years in some cases. These reservoirs have likely been sequestered from exchange with the atmosphere due to a dust/debris cover and have contributed little to global cycles for long periods (Toon et al., 1980; Bramson et al., 2017).

1.2.4. Climate models and PLD formation

1.2.4.1. Introduction and methodology. Models are critical tools for investigating the past climate of Mars, and global climate models (GCMs) have been used to study aspects of the Amazonian (last ~2.8 Gyr of Martian history) climate and the formation of the PLDs. Since the Amazonian period is characterized by a solar luminosity similar to the current solar luminosity and an atmospheric mass comparable to what it is today, we can study the climate by considering how changes to the orbital parameters would affect the present-day Mars climate. Thus, the general methodology for these studies is to execute a GCM that does a reasonable job of reproducing the current Mars climate with modified orbit parameters (obliquity, eccentricity, argument of perihelion).

1.2.4.2. Modeling the current climate. The cycles of CO_2, dust, and water, including sublimation and deposition, dominate the climate of Mars. The GCM community has invested significant effort over the past few decades towards improving how GCMs handle and predict these cycles. This requires the implementation of a wide range of physical processes that govern how dust, CO_2, and water cycle into, through, and out of the atmosphere considering surface and orbital properties.

CO_2 is the most straightforward cycle to simulate. Surface energy balance methods are used to compute CO_2 condensation and sublimation as CO_2 cycle into and out of the seasonal CO_2 polar caps. Atmospheric condensation of CO_2 is usually handled with a simple scheme in lieu of representing the more complex microphysical processes of cloud formation (Forget et al., 1999; Haberle et al., 2008; Guo et al., 2009), and recent work has improved how CO_2 clouds are simulated in GCMs (Listowski et al., 2013; Dequaire et al., 2014).

Significant effort has been invested in improving the handling of water cycle physics in GCMs (Fig. 5) based on modern observations. Even though there are other contributors, in modeling, the NPRC and NPLD outliers are generally considered to be the primary source of water to the present atmosphere (Navarro et al., 2014), but investigations may include a regolith source (Böttger et al., 2005) that accesses ancient ice deposits. Sophisticated microphysical schemes can explicitly include the physics of nucleation, growth, and size-dependent sedimentation (Montmessin et al., 2002, 2004). The inclusion of cloud radiative effects has proven quite challenging due to the many complex feedbacks involved, but significant progress has been made in realistically representing the seasonal cycles of water vapor and clouds (Navarro et al., 2014; Haberle et al., 2018).

The dust cycle remains the most challenging of the three climate cycles to simulate fully. Investigations that include the physics of dust

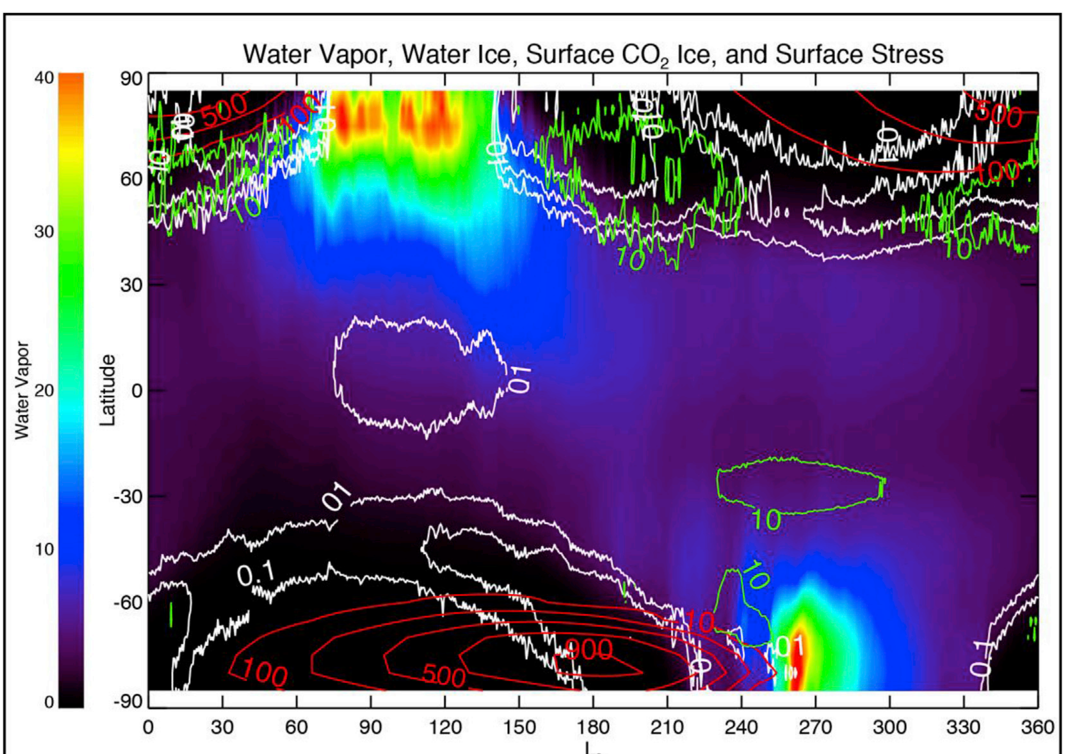

Fig. 5. Current-day seasonal cycles by latitude and season of atmospheric water vapor (color fill), atmospheric water ice (white contours), surface carbon dioxide ice (red contours), and surface stress (green contours) as simulated by the NASA/Ames Legacy Mars GCM.

lifting based on resolved surface wind stress and dust devils (and/or unresolved small-scale lifting) can capture general behaviors of the observed dust cycle but are thus far unable to realistically simulate others (Newman et al., 2002; Basu et al., 2004; Kahre et al., 2006). In particular, capturing the observed inter-annual variability of global dust storms remains elusive. In lieu of using fully interactive methods, studies that focus on other aspects of the martian climate generally use prescribed or semi-prescribed dust methods based. In these studies, the horizontal and/or vertical distribution is constrained by observations (Montabone et al., 2015). Caution is warranted when using the dust observations for past climate studies because it is unlikely that the seasonal patterns of atmospheric dust remain the same as orbit parameters change.

1.2.4.3. Current understanding of amazonian climate. Modeling the Amazonian climate involves running GCMs that are generally capable of capturing the main components of the current Mars climate for different orbit parameters. Because GCMs are complex and require significant computational resources, it is not possible to explicitly simulate changing orbit parameters. Instead, combinations of obliquity, eccentricity, and season of perihelion are chosen to map out trends and branch points in the behavior of the climate. When designing these simulations, the total inventories and available surface reservoirs of CO_2, dust, and water must be considered. The effects of increasing or decreasing the obliquity are generally more substantial than changing the eccentricity or season of perihelion (Laskar et al., 2004).

Obliquity variations have important consequences for the CO_2 cycle. As obliquity increases, the annual mean insolation at the poles increases. For obliquities greater than 54°, the poles receive more annual insolation than the equator. This drives more extreme seasonal variations in surface temperature and surface CO_2 ice. Overall, the global average surface pressure decreases with increasing obliquity because more CO_2 cycles into and out of the polar ice caps seasonally (Mischna et al., 2003; Haberle et al., 2003; Newman et al., 2005). At low obliquities ($<\sim 20°$), permanent CO_2 ice caps form and the atmosphere collapses (Haberle et al., 2003; Newman et al., 2005; Manning et al., 2006, 2019; Buhler et al., in press). In a collapsed state, the equilibrated atmospheric mass could be quite low (~30 Pa). Recent models have begun considering what would happen if the $\sim 2.6 \times 10^{16}$ of CO_2 locked in the south pole (Phillips et al., 2011) were available to circulate through the atmosphere.

At low obliquities (<30°) when the polar insolation is low, water ice is stable at the pole and the atmosphere is relative dry (Mischna et al., 2003; Forget et al., 2006; Levrard et al., 2007). The hemisphere where the polar water ice resides is likely controlled by the season of perihelion, with the north favored when the perihelion occurs near southern summer solstice and the south favored when perihelion occurs near northern summer solstice (Montmessin et al., 2007). At moderate obliquity (30–40°), water ice becomes stable in the middle latitudes and the atmosphere is considerably wetter (Madeleine et al., 2009). At high obliquity, water ice is destabilized from the poles and becomes stable at low latitudes (Mischna and Richardson, 2005 Forget et al., 2006; Levrard et al., 2007). The radiatively active ice clouds have significant effects, particularly at moderate to high obliquity. Models predict that optically thick clouds form up high, which allows them to significantly warm the surface, enhance the mean circulation, and produce significant snowfall (Haberle et al., 2012; Madeleine et al., 2014; Kahre et al., 2018).

From the subsurface, water ice may interact with the atmosphere, and varying orbital parameters controlling insolation will drive transport between the poles and mid- or low-latitudes. This is modulated by slope and thermal lags. Presently, mid-latitude deposits that should not be stable likely exist because of a protective lag (Bramson et al., 2017).

As obliquity increases, the Hadley cell is enhanced due to an increased equator-to-pole temperature gradient. The stronger return flow from the overturning circulation increases surface stress and thus wind-stress dust lifting (Haberle et al., 2003). Once dust is lifted, positive radiative/dynamic feedbacks further enhance the Hadley cell and dust lifting (Newman et al., 2005). While this predicted behavior is robust, there are potential caveats that must be considered. The first is the incorrect assumption that an infinite amount of surface dust is available for lifting everywhere on the planet. The second caveat is that early dust cycle simulations at high obliquity did not include water ice clouds. Clouds can scavenge dust and provide additional radiative/dynamic feedbacks that need to be fully understood.

1.2.4.4. Modeling the polar layer deposits. The PLDs contain a record of the martian climate over time, so realistically modeling this record will require the use of models that are capable of creating an evolving climate state and potential for internal deformation of ice. While there have been some attempts to use results (or general behaviors) from GCMs to model the PLDs, this process has proven very challenging due to the complexities of the processes involved.

In the most comprehensive effort, Levrard et al. (2007) predicted polar ice deposition and removal rates over a range of obliquities taken from the computed obliquity history of Laskar et al. (2004) over the past 10 million years. They quantitatively tracked the evolution of polar surface ice reservoirs and found that the north cap could begin accumulating about 4 million years ago (Fig. 4). The model predicted ~30 layers that could have been generated by the changing obliquity during the past 4 million years. This number is inconsistent with thousands of visible layers of the NPLD but similar in order to the number of radar reflectors observed. This result implies that visible dusty layers form on a shorter time frame, perhaps related to precession of the argument of perihelion, which should modulate layer formation. However, that study did not use a model with an interactive dust cycle or radiatively active clouds, two major factors required for any successful climate modeling of Mars, especially since the amount of dust deposited in the polar regions could vary significantly with varying orbital configurations (e.g., Newman et al., 2005). Fully coupled dust and water cycle simulations will further our understanding of how the PLDs have formed due to orbit-driven variations in the martian climate (e.g. recently presented work by Emmett and Murphy (2018)).

1.3. History of mars polar investigations

1.3.1. Orbiters

Spacecraft investigations of the polar regions of Mars began with the Mariner 7 flyby in 1969 when the infrared spectrometer observed CO_2 ice, related to seasonal processes (Herr and Pimentel, 1969). Imagery of the polar regions began in 1971 with Mariner 9 and continued with the comprehensive coverage by Viking orbiters (1976–80). In the modern era, imagery at ever increasing spatial resolution has been obtained from the Mars Global Surveyor (MGS), Odyssey, Mars Express, and Mars Reconnaissance Orbiter (MRO) orbiters using the High Resolution Stereo Camera (HRSC), MOC, THEMIS, CTX, and HiRISE instruments. Infrared observations to observe surface properties began with multi-channel instruments (Infrared Thermal Mapper (IRTM) on Viking) and advanced to full spectroscopy and compositional measurements with the MGS Thermal Emission Spectrometer (TES), Mars Odyssey's THEMIS, and continues with Mars Express' Observatoire pour la Minéralogie, l'Eau, les Glaces et l'Activité (OMEGA), and MRO's Compact Reconnaissance Imaging Spectrometer for Mars (CRISM). Infrared spectroscopy began with the Infrared Interferometer Spectrometer (IRIS) instrument on Mariner 9 and continued with MGS′ TES, Mars Express' Planetary Fourier Spectrometer (PFS), and MRO's Mars Climate Sounder (MCS) (e.g. Smith, 2008). Gamma ray and neutron spectroscopy on Odyssey has been used to study ice (Feldman et al., 2002), and laser altimetry from the Mars Orbiter Laser Altimeter (MOLA) has been used to estimate the total thickness of the PLD and measure seasonal elevation change with deposition (Smith et al., 2001). Radar measurements to probe the subsurface have been performed from both MARSIS and SHARAD sounders (Picardi et al., 2004; Seu et al., 2007).

Polar studies have benefitted from several kinds of orbital observations. Optical and infrared instruments tracked stratigraphy, geomorphology, seasonal geologic processes, inter-annual variability, composition, albedo, and physical state of H_2O and CO_2 ice deposits. Spectrometers track grain size and layer properties on the surface (Calvin et al., 2009; Brown et al., 2016) along with the distribution of hydrated materials, altered glasses and basaltic materials, and the origins of gypsum on the north polar dunes (Langevin et al., 2005; Horgan et al., 2009; Horgan and Bell, 2012; Massé et al., 2012). Instruments that measure atmospheric properties tell us about thermal and humidity profiles, cloud formation, and snowfall (Hayne et al., 2014). Temperature sensing instruments tell about the thermal inertia of ice-cemented material or the PLD (Putzig et al., 2014). Finally, orbital radars have been instrumental in determining the bulk dielectric properties of the PLD and 3-D stratigraphic relationships inaccessible with cameras.

1.3.2. Landers

The polar regions of Mars have been a high-priority target for landed missions for decades. Since their discovery in Mariner 9 images (Murray et al., 1972), the polar layered deposits were suggested to contain a climate record, which could be accessed in at least a limited number of exposures (Cutts, 1973; Howard et al., 1982). High-resolution images from MOC revealed much more extensive layered deposits than had been previously recognized, especially in the south polar region (Malin et al., 1998).

Mars Polar Lander. Landing site selection for NASA's Mars '98 mission was guided towards the south polar deposits, where remote sensing data revealed a vast volume of ice just beneath a layer of dust or regolith. This mission became Mars Polar Lander, which had primary science objectives to dig into the subsurface to search for water, to measure the atmospheric composition, and to survey the SPLD to better understand their formation mechanisms. Its landing site was located in a region between 73 and 78°S and 170–230°W. In addition to the main lander, the Mars Polar Lander spacecraft also contained two penetrator probes, called Deep Space 2 (DS-2) designed to sample the atmosphere during descent, and the subsurface soil and ice layers following impact. Unfortunately, a malfunction in the Mars Polar Lander's descent stage caused the catastrophic loss of both the primary payload and DS-2 (Albee, 2000).

Phoenix. Resurrected as the Phoenix mission, the 2001 Surveyor Lander was repurposed to a high latitude location. Launched in 2007, Phoenix landed at a position of 68.22° N, 125.7° W on May 25, 2008. Its primary purposes were to study the geologic history and habitability of subsurface water by sampling material at this high-latitude landing site and collect data on how the Martian climate is affected by polar dynamics.

Although its location was over 700 km from the NPLD, the Phoenix mission's landing site was on top of a region with well-established ground ice, where remote sensing and model calculations had shown ice likely to be present in the upper few centimeters (Fanale et al., 1986; Mellon and Jakosky, 1993; Feldman et al., 1993; Aharonson and Schorghofer, 2006; Putzig and Mellon, 2007; Mellon et al., 2008). Indeed, the landing thrusters revealed a patch of ice under the lander, and the robotic arm and scoop excavated ice beneath a layer of loose, ice-free soil ~5 cm thick (Mellon et al., 2008). Wet chemistry measurements of soils revealed salts, including perchlorate (Hecht et al., 2009), which are freezing point depressants for water. Significant exchange of water vapor between the surface and atmosphere was detected by the lander's Thermal and Electrical conductivity Probe (TECP; Zent et al., 2018).

1.3.3. Previous concept studies

In the past four decades, numerous missions to the northern polar deposits have been proposed as part of either concept studies or spacecraft proposals. Perhaps the earliest concept was described shortly after the first Viking landing (Staehle, 1976; Staehle et al., 1977). None passed beyond the proposal stage. A subset, from the last 15 years, is summarized here to represent past polar community thinking on observational strategies. One can see that while the technology and exploration platforms have varied, the core observational strategies desired by the polar community have not.

1.3.3.1. Decadal Survey concept studies. In a mission concept study associated with the SS2012 Planetary Science Decadal Survey, Calvin et al. (2010) identified how to use the following basic architectures for near-future polar missions: Discovery-class orbiters, New Frontiers-class orbiter, Discovery-class lander, New Frontiers-class lander, and New Frontiers-class rover.

Discovery and New Frontiers-class orbiters would focus on global climate and seasonal processes, surface energy balance and composition, and atmospheric sounding. Discovery and New Frontiers-class landers have been conceived and proposed to perform cm-scale stratigraphic analysis and surface-atmosphere interactions on ~1 Mars year time scales. Meteorologic packages would be included. Options range from landing at the base of a polar scarp to subsurface access with drills or high-resolution radar remote sensing. New Frontiers-class rovers have also been conceived that would carry a rock corer or drill to collect samples for analysis through traversing across exposed layers. Analysis would have greater coverage than a static lander. Smaller rovers that arrive as part of a larger platform have also been studied. The strawman payload included an imager; navigation cameras; tunable diode laser spectrometer (for distinguishing the various water isotopes); microscopic imager, Raman spectrometer, and chemical sensors.

Drilling may be done in multiple ways. Three mission concepts used a thermal energy source to melt water and descend into the melt hole. Analysis of the interior of the polar deposits must be done on the walls of the hole as the drill descends using instrumentation fit within the thermal drill itself, or upon the resulting meltwater pumped through the tether to an instrumented surface platform. Concepts include Cryoscout (Zimmerman et al., 2002; Hecht and Saunders, 2003), CHRONOS (Hecht, 2006), and Palmer Quest (Carsey et al., 2005a, 2005b), a NASA Vision Study. Instruments for those landed studies included the following to go into the bore hole: nephelometer for recording visible stratigraphy in full color; electrochemical sensors for salt composition; laser hygrometer for H and O abundance; temperature sensors; seismometer. On the surface, a stereoscopic imager; meteorologic package; laser spectrometer; and electrochemical sensors.

While none of the mission concepts outlined above made it past (or in some cases, to) the proposal stage, common themes of exploration are clear: accessing the local subsurface stratigraphy, placing it in the regional context of the broader polar deposits, assessing the atmosphere above the surface, and relating it to the seasonal evolution of the polar surface.

1.4. Terrestrial climate studies using ice cores

Terrestrial glaciers and ice sheets provide accessible field sites that can support our understanding of local processes that relate to those on Mars. Terrestrial ice represents a key component of the Earth climate system and interact dynamically with climate through several different processes. During glacial cycles, growth and retreat of glaciers in the northern hemisphere enhances the effects of climate changes through the ice-albedo feedback (Ruddiman et al., 2006). In the present warming climate, surface melting and mass loss is further enhanced during summer due to the darkening effect of meltwater and dust at the surface of retreating glaciers and ice sheets (Tedesco et al., 2016). Increased discharge from marine terminating glaciers due to warm ocean temperatures may subsequently influence ocean circulation with global effects (Vaughan et al., 2013). Three key themes related to terrestrial glaciers and ice sheets stand out in modern terrestrial climates studies: understanding drivers of the glacial cycles of the Pleistocene (past ~2.6 Myr), deriving the paleo-climatic history from the ice core archives, and estimating the mass loss from glaciers and ice sheets and their contribution to global sea level.

1.4.1. The general flow pattern of ice sheets

On Earth, ice sheets form when climate conditions allow snow to accumulate at the surface over thousands of years, and they initiate and grow from mountainous areas that are colder than lower elevations (Cuffey and Paterson, 2010; Hvidberg et al., 2013). In the large terrestrial ice sheets, ice accumulates in the interior by snowfall, ice flows slowly towards the margin as the ice sheets spread due to gravity, and ice is lost along the margins by surface melting and run off or by discharge into the ocean from marine terminating glaciers. Although ice sheets respond to climate changes, they may gradually reach a steady state where snow accumulation is approximately balanced by discharge and runoff. In the high-elevation interior, the ice sheets are more than 3 km thick. There, layers are compressed and deform as they gradually sink into the ice sheet and flow. Climate proxies from ice cores drilled through these layers need to consider the thinning and stretching of the layers due to flow.

1.4.2. Transformation of snow to ice

Freshly deposited snow in the interior of the Greenland or Antarctic ice sheets has a density of 300–400 km m^{-3}. Density variations in the top tens of meters of the snowpack (firn) reveal an annual stratigraphy due to temperature and impurity content as well as individual events, e.g. wind crusts formed by packing action of wind. Within the top 60–120 m, the firn gradually transforms vis sintering into glacier ice with a density of 830 km m^{-3} (Sowers et al., 1992; Gow, 1969). Flow and compaction of air bubbles below the firn-ice transition increase the density further to 920 km m^{-3}. Deeper ice does not densify further. The depth of the firn-ice transition depends mainly on the mean annual temperature and rate of snowfall and can vary from 70 to 100+ m. Glacier ice contains air bubbles with samples of the atmosphere from the time of the bubble close off and are used to document variations in past atmospheric composition (Cuffey and Paterson, 2010).

1.4.3. Composition, stratigraphy and timescales

Terrestrial ice sheets generally consist of nearly pure water ice with a small impurity content (Fig. 6). Impurities originate from aerosols or particles deposited with the snow (Fig. 7, top). Impurity records have an annual variation related to the atmospheric circulation and transport or are related to specific events, e.g. volcanic eruptions or forest fires. The stratigraphy in ice cores is observed by the electrical conductivity measurement (ECM) and dielectrical profiling (DEP), by continuous high-resolution profiles of concentrations of chemical impurities using the continuous flow apparatus (CFA) method, or by concentration of dust particles (e.g. Svensson et al., 2008; Cuffey and Paterson, 2010). ECM is a measure of the acidity of the ice and used to identify volcanic reference horizons due to their high concentration of sulfuric acid, and climate transitions due to the shifts in impurity concentrations and thereby changes in conductivity. CFA provides multiple continuous records of impurities and thereby allows identification of annual layers. In Greenland, the annual accumulation rate is sufficiently high to preserve an annual signal, and it is possible to detect the seasonal cycle in several impurity concentration records, e.g. insoluble dust, Ca^{2+}, NO_3, ECM (Svensson et al., 2008). Insoluble dust particles from continents are carried by winds through the troposphere and deposited over the ice sheets. The particles typically have a size of order 0.1–2 μm and a bulk dust concentration of 50–200 μg per kg of ice in the interior of Antarctica and Greenland, respectively (Lambert et al., 2008; Steffensen et al., 2008). During glacial periods, the concentration of continental dust increases by a factor of 10–100 (Greenland) and a factor of 20–50 (Antarctica). In Greenland, the dust concentration in glacial ice is high enough to influence the crystal size, and layers of high dust concentration are associated with small crystals. Crystal size is generally in the order of 0.1–1 cm^2 and increases with depth but drops at the Holocene-Pleistocene transition with a factor of 2. Although the dust is not visible by itself in the glacial ice, dust-rich layers can be identified in the visible stratigraphy of ice cores as cloudy bands. The visible stratigraphy in Greenlandic ice cores has revealed annual layers in the glacial ice down to a resolution of 1 cm (Svensson et al., 2005).

Fig. 6. Ice core from 1 km depth of the East Greenland Ice-core Project (EastGRIP) core in. For most cores in Greenland layers are not visible to the eye, and other methods must be employed to characterize them. Photo by C. Hvidberg.

In Greenland, ice cores have been dated accurately by layer counting back to 60 kyr ago using a combination of visible stratigraphy, concentration of dust and chemical impurities (Svensson et al., 2008). In the interior of East Antarctica, the annual accumulation is only few centimeters and annual layers cannot be identified. Ice cores in East Antarctica are dated from a combination of reference horizons with dates transferred from Greenlandic ice cores or other paleoclimatic records and ice flow modeling, taking into account thinning of layers due to flow and using consistent relations between climate and snow accumulation rate (Veres et al., 2013).

1.4.4. Radar stratigraphy

As on Mars, radar sounding is used to map the stratigraphy of terrestrial ice sheets. The stratigraphy in the top tens of meters is mapped with higher-frequency snow radar systems, employed from the air or the surface with ground penetrating radar (GPR) systems. The snow structure of the dry snow zone in Greenland has for example been mapped with an airborne Ku-band synthetic aperture radar (SAR) system and linked to in-

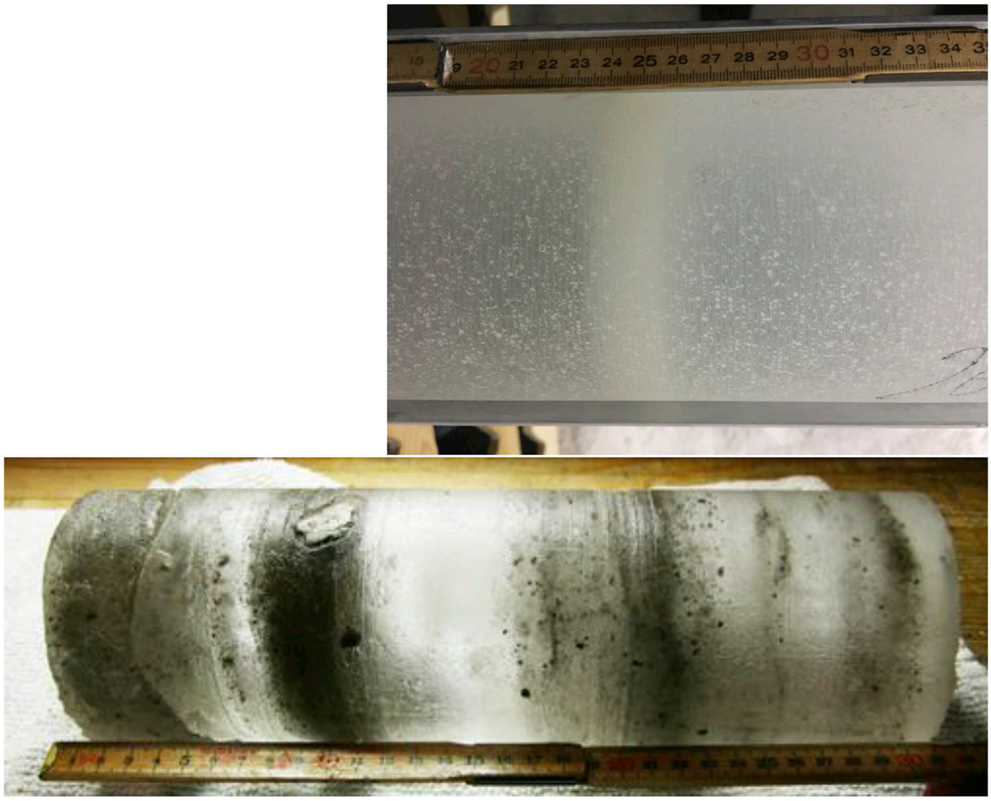

Fig. 7. Examples of visible layering in the North Greenland Eemian Ice Drilling (NEEM) ice core. Top: This layer is one of the only major, visible ash layers in Greenland; most are much thinner. Bottom: Layers of rocks and grains in the bottom tens of cm of the 2537.36 m deep NEEM ice core. Large grains are not found above the lowermost section. Photos by C. Hvidberg.

situ observations from shallow ice cores and pit studies. The observations reveal the annual layer structure in the top 15–20 m related to density variations in the firn, which forms due to seasonal variations in temperature, snowfall and impurity concentrations.

The internal radar layers show the past surfaces of the ice sheet as they sink down and are subject to flow, including thinning and stretching, local variations of basal melting, and large-scale evolution of the ice sheet and its flow pattern. Repeated surveys over several years show how layers sink into the ice sheet and new layers form at the surface and allow detailed mapping of spatial and temporal variations of the annual snow accumulation (e.g. Simonsen et al., 2013). Medley et al. (2014) has performed an Antarctic counterpart to the Greenland surveys, and Koenig et al. (2016) have performed a more recent and more extensive survey that improves temporal and spatial resolution.

In general, the radar stratigraphy of ice sheets arises from transitions in the bulk electrical conductivity of the media due to density variations, volcanic reference horizons, ice crystal structure, or climatic transitions associated with changes in impurity concentration of the ice. Deep internal radar layers have been linked to ice cores and dated using ice core timescales in Greenland and Antarctica (e.g. MacGregor et al., 2015; Winter et al., 2017). In Greenland, they are associated with abrupt climate transitions during the last glacial, known as Dansgaard-Oeschger cycles, or with glacial-interglacial transitions. In both Greenland and Antarctica, echo-free zones occur; however those have now been partially attributed to lack of signal power (Winter et al., 2017), and new radar systems are capable of resolving deep layers there too. In Greenland, ice that deposited during the last glacial maximum, between ~15 and 30 kyr, contain no distinct radar-echo layers, possibly due to a generally high level of continental dust ($CaCO_3$ and Ca^{2+} ions), which neutralizes any volcanic acidity peaks during that period. The oldest ice in both Greenland and Antarctica are echo free or have a few blurred layers, and here it has been suggested that flow effects in these deep and old layers could have smeared out the transitions, e.g. by thinning layers or shearing and folding layers of different rheology (NEEM NEEM Community members, 2013).

1.4.5. The climate archive in ice cores

Paleo-climatic records from terrestrial ice cores have revolutionized the understanding of the Earth climate history and, together with ocean sediment cores, provided knowledge of glacial cycles and beyond. The key contributions of ice cores to the paleoclimatic community are their accurate and independent timescales as well as the unique information of past temperatures from oxygen isotopes (e.g. $\delta^{18}O$ and δD) and past atmospheric composition from air trapped within the ice (e.g. CO_2, CH_4) (Cuffey and Paterson, 2010). The ability to detect annual variations in many different parameters, such as oxygen isotopes, insoluble dust, and chemical impurities - and thereby identify and count each year - has contributed to understanding the timing and phases of climate changes in the past. Terrestrial ice cores contain an undisturbed stratigraphic record of ~100 kyr (Greenland) and ~1 Myr (Antarctica) (Cuffey and Paterson, 2010). Older layers are disturbed by flow or removed by basal melt. The climate archive of terrestrial ice cores is continuously expanded with new climate proxies and new techniques that make it possible to detect more parameters and reduce sample size. One example is CFA. Ice is continuously melted along the ice core and analyzed in a semi-automatic wet-chemistry lab to provide records of isotopes, ions, cations, insoluble dust particles, conductivity, black carbon, etc., that contain information about atmospheric and oceanic circulation patterns, sea ice conditions, forest fires, far-field humidity, etc. The interpretation of these proxy records is done in combination with climate modeling and paleo-climatic records from other archives.

1.4.6. Selection of the drill site and recommendations for Mars

Ice cores from the interior Greenland and Antarctica are widely used to infer the climate history of Earth because the timescale is reliable, and the records have been interpreted to provide the hemispheric or global climate history (e.g. EPICA EPICA community members, 2004; NEEM NEEM Community members, 2013). The ice core records contain continuously deposited layers and allow age determination from measurements of constituents known to vary on annual timescales combined with reference horizons known from other stratigraphic records. Comparisons between ice cores spaced over tens of meters show significant local variations in snow accumulation rate due to surface roughness and wind effects, where snow is redistributed at the surface or removed due to wind scouring, but decade-averaged records are similar. Radar stratigraphy from the top meters of the firn to the deep (2–3 km) layers are continuous and smoothly varying and show similarly that the stratigraphy of the large ice sheets represents large-scale climate variations in the past, not local snow accumulation patterns (MacGregor et al., 2015).

Prior to an ice core drilling program, data are collected from the area and used for the drill site selection and planning of the campaign (e.g. Dahl-Jensen et al., 2002). Surface campaigns and radar surveys provide information on annual snow accumulation rate, ice thickness, ice flow velocity, surface conditions and local weather, as well as internal layer structure. In general, sites are preferred with the following qualities: smooth bedrock, unfolded internal layers, no signs of basal melting or complicated flow over complex underlying topography (e.g. mountains), only little horizontal movement, with cold surface conditions, and no melting at the surface or at the base. The optimal site has undisturbed layers and no complicating upstream conditions.

2. Major questions to address and key measurements

2.1. Major science questions and objectives

Based on existing knowledge and knowledge gaps that need to be bridged, the KISS workshop members listed numerous questions yet to be answered. Many shared a theme, and taken together four overarching questions about the climate record stored in the PLD:

1. What are present and past fluxes of volatiles, dust, and other materials into and out of the polar regions?
2. How do orbital forcing and exchange with other reservoirs affect those fluxes?
3. What chemical and physical processes form and modify layers?
4. What is the timespan, completeness, and temporal resolution of the climate history recorded in the PLD?

We refer to these questions as, "**Fluxes**," "**Forcings**," "**Layer Processes**," and "**Record**," and in this section we discuss the value of answering each.

2.1.1. Fluxes

2.1.1.1. Observations. Measuring the modern-day fluxes of volatiles, dust, and other materials from lower latitudes to the polar regions and then onto the polar caps are key steps to interpreting the climate record in the PLDs. Obtaining these measurements would provide the opportunity to link observable modern climatic processes to material arrival at the PLD surface, leading to individual layer formation (Section 2.A.3) and to connect to the polar geologic record (Section 2.A.4). We expect that variation in the isotopic and chemical composition and total mass of material exchanging between the atmosphere and polar deposits will yield observable signals in the PLD. Therefore, we focus our attention on measuring these quantities and on quantifying the atmospheric processes that govern these fluxes. To do this, we must measure fluxes at global and regional scales and the exchange between the surface and atmosphere. Four categories of material exchange annually between the atmosphere and the polar deposits. In order of decreasing quantity by volume or mass they are CO_2, H_2O, refractory materials (e.g. dust, salts, volcanic debris, hydrocarbons), and trace volatile species. One big uncertainty is the source reservoirs of these materials, which may have formed in different epochs and contain variable inputs to the current climate, so observations that track the locations of these materials spatially are critical inputs to our modern climate understanding.

The largest component of the gross annual flux is CO_2 (Leighton and Murray, 1996) which in condensed form reaches several hundred kg m^{-2} over the PLD. However, orbital observations show that annually, there is no net flux of CO_2 onto the north polar cap and the mass balance of the SPRC cannot be determined better than ±1 kg m^{-2} per martian year (Thomas et al., 2016). Additional measurements of surface pressure from landers cannot detect a secular change in pressure that would imply net mass change at the SPRC (e.g. Haberle and Kahre, 2010). Nevertheless, measuring the relative proportion of winter CO_2 laid down through direct deposition vs. snowfall is important because these different modes lead to vastly different thermal, radiative, and structural properties (e.g. Colaprete et al., 2005). This will affect the incorporation of co-deposited material into the polar caps. Additionally, measuring seasonal isotopic variation (e.g. Villanueva et al., 2015) during deposition and sublimation of CO_2 will aid in the interpretation of the isotopic abundances of trapped gas within the PLD.

The flux of H_2O relative to that of refractory materials under modern climatic conditions is a key measurement for deciphering what goes into layer formation and for determining the climatic signal of variable dust fraction stored in the PLD. Measurements from orbit can track dust movement towards the polar regions, and surface measurements can determine how much of that falls to the surface either directly or is scavenged to make snow. In addition, knowledge of the chemical and isotopic composition of this material will yield important information, such as the reservoir provenance for dust or ice (Vos et al., 2019). Seasonal isotopic variability in the H_2O flux, including D/H, would come from a combination of mass-dependent fractionation or changing source reservoirs, and solar activity may influence D/H ratios on longer time scales (Fisher, 2007). This may be used to interpret H_2O isotopic variation recorded in the PLD, and the current state is critically unconstrained. Importantly, this isotopic variation may be annual and may provide the smallest resolvable cyclic signal in the PLD. Finally, the flux of trace volatiles incorporated into the polar cap compared to the ambient trace volatile composition will support deciphering trapped atmospheric gas bubbles in the PLD. Several measurements are necessary in order to understand the fluxes of material at all scales:

- Wind speed profile near the surface boundary layer. Near-surface wind speed is determined by nonlinear processes that are impossible to model *a priori.* When observed concurrently with the number density of atmospheric refractory material and H_2O, this is a basic input for calculating regional flux.
- Horizontal and vertical wind speeds globally and over several Mars years. This will be used to validate GCMs and track movement of dust and other tracers. Tellingly, wind speeds have never been systematically measured globally that include the full boundary layer.
- 4-dimensional (altitude, latitude, longitude, and time) number density map of atmospheric dust and H_2O. The ideal minimum resolution for these measurements is a 10-point vertical grid within the first half-scale height (scale height is ~11 km) and half-scale height resolution up to 80 km, at a 4x diurnal cadence, resolved across 12 longitudinal bands, all observed over one full martian year. Isotopic measurements of H_2O (e.g. D/H, $\delta^{18}O$, $\delta^{17}O$) are also important for tracking its provenance. Combined with wind speed, the number density of material is a basic input for calculating regional flux.
- *In situ* surface mass flux of H_2O, refractory material, and CO_2. It is most critical to obtain this measurement at one well-selected location; however, additional measurement locations would allow the determination of regional variability. Characterizing the chemical and isotopic makeup of the surface material is also desirable for

determining the provenance of the fluxing material and connecting *in situ* measurements to global measurements.
- Obtaining surface and orbital measurements concurrently is important for accurately determining fluxes and connecting local deposition to global climatic processes.

2.1.1.2. Modeling. Atmospheric models will be used in conjunction with observations to quantify the fluxes of non-volatile and volatile material into and out of the polar caps on Mars. Two steps are necessary. The first is that models require observations for validation purposes. Second, models will be invaluable tools for interpreting and expanding the observations beyond measurements.

2.1.1.2.1. Model validation. Before models can be reliably used to extrapolate information gained from one or a few locations to the entire polar cap region, they must be validated with observations. Winds and turbulence in the lower atmosphere control the exchange of volatiles and dust between the surface and atmosphere and transport those materials. However, to date, these processes have not been comprehensively or reliably measured on Mars. Near surface wind measurements have been acquired by the Viking Landers, Pathfinder, Phoenix, and Curiosity but these data sets suffer from calibration issues and other problems. The Interior Exploration using Seismic Investigations, Geodesy and Heat Transport (InSight), recently landed on Mars, is providing an improved look at pressure and wind speeds at one low latitude location.

Winds above ~1.5–2.0 m have never been directly measured on Mars apart from a few entry, descent and landing profiles. Instead, our understanding of the winds throughout the bulk of the atmosphere have come from deriving thermally balanced winds from observed thermal structures and atmospheric models (Navarro et al., 2017). Models require wind observations for validation, particularly near the surface where the thermal wind balance approximation cannot be used. Well-calibrated measurements of near-surfaces winds or wind profiles from the surface in conjunction with global wind speed measurements from orbit will provide this critical model validation. In addition to wind observations, direct observations of the rates of exchange of dust and volatiles between the surface and the atmosphere in the polar regions will provide critical constraints for models. Current state-of-the-art global- and regional-scale models include the physics of dust lifting and removal, and water and CO_2 ice sublimation, deposition, and snowfall. In the absence of measurements of the fluxes from each process, however, it is difficult to know if the models are handling these processes correctly.

Once models are fully vetted for present day processes, their value in representing past behavior grows. At that point, we will be in a much better position to understand how orbital parameters and other forcings (Section 2.A.2) affect the recorded climate signal (Section 2.A.4).

2.1.1.2.2. Interpreting/expanding observations. We expect significant spatial and temporal variations in the surface fluxes of dust and water over PLDs due to regional and local-scale circulations and spatial variations in surface properties. It would be optimal to have a large network of highly capable meteorological stations placed strategically around the polar regions. Barring that, models will be critical tools for extrapolating information from a small number of stations to a comprehensive understanding of what is occurring over the entire region. Additionally, unless there are observations from orbit of the global transport of dust and volatiles concurrent with *in situ* measurements, global-scale climate models will likely be needed to provide this global perspective.

2.1.2. Forcings

2.1.2.1. Observables in the PLD and climate signal. In order to determine the forcings that create the volatile deposits, *in situ* measurements of the layers of the PLD must be made. The materials to be measured are discussed in section 2.A.4. By measuring observables in a stratigraphic column, we can track the variability at each layer, going backwards in time. If those variables are cyclical in nature, then perhaps we can tie those signals to the periodic nature of seasonal or annual cycles, dust storms, solar cycles, and longer period cycles driven by orbital changes. Correlating time-series or possible forcings to stratigraphic measurements will test our hypotheses about the orbital evolution of Mars.

Part of understanding forcings is to learn how off-polar volatile reservoirs respond to changes in orbital parameters. In order to do this, the first step is to characterize and inventory all off-polar reservoirs. Secondly, many are meta-stable in the current climate, so discovering the processes that stabilize these reservoirs and how that responds to changing insolation is critical.

2.1.3. Layer-formation processes

Modern processes related to layer formation are not well known, and yet the materials from the present surface will one day become incorporated into the PLD. Reading the variability in layer composition through time requires an understanding of what goes into making a layer today. Importantly, layer formation doesn't end upon burial. Communication with the atmosphere occurs down to an unknown depth; cosmic radiation interacts with materials; and chemical or physical forces can recrystalize the ice and exclude or incorporate impurities. Thus, determining all of the processes that affect layers is a critical knowledge gap, and measurements on the surface will determine what products form on the surface and remain in the ice or decay.

To measure modern processes, we need access to the surface and the upper 50 cm away from an outcrop. 50 cm is significant because the processes described above have likely fully ceased by this depth, so it will be possible to extract the necessary information without worrying about missing processes. Additionally, based on estimated accumulation rates (Becerra et al., 2017a, 2017b and references within), 50 cm is expected to represent the last 1000 years of Mars history, a period in which the climate should have been nearly identical to present day. Thus, it will be possible to measure layer formation without complications from variable inputs.

Composition was identified as the top priority because it closely links to the climate record (Section 2.A.4) and is informative about fluxes of materials to the poles (Section 2.A.1) by identifying potential sources of materials that make up the layers. The relative abundances of the highest concentration constituents (water ice, dust, and salts) will be key for investigations on these topics. Identifying trace quantities of other materials (e.g. organics, isotopes, clathrate) and identifying composition at multiple spots (if landed) or better vertical resolution than currently available (from orbit) are also important. These observations will require an instrument capable of identifying and measuring different constituents to high precision. Next, an improved understanding of layer formation processes in the recent past (top 50 cm) will then allow us to compare to deeper and older layers exposed at trough outcrops.

Ice microstructure is important for determining the physical properties of the NPLD. Phase partitioning of salt and impurities from ice grains is likely to be different on Mars because of the materials involved. Density and grain size distribution of dust can tell us of source material and perhaps past atmospheric states. These properties affect layers and the strength of NPLD materials. Measuring the distribution of components within layers will provide important information about how the layers of the NPLD respond to forces.

The study of current surface and meteorologic processes will illuminate how material becomes available for layer formation or removed from the system. Meteorologic measurements at the surface will be compared to global and regional measurements (Section 2.A.1) in order to determine the availability of material through the present epoch. Then, in combination with GCMs, we can estimate the availability of material and forcings that formed past layers (Section 2.A.2). Similar to layer formation, measuring meteorological processes requires *in situ* observation over an entire martian year. Measurements within a single site and across many sites should be simultaneous to gain the most value. They should include the ablation and/or accumulation of dust and ice (H_2O and CO_2), saltation and surface transport of materials, wind speed, insolation, humidity, temperature, pressure, and albedo.

2.1.4. Record

In order to address the science question "What is the timespan, completeness, and temporal resolution recorded in the PLD?" we identified three time (and size) scales that need to be addressed. The largest physical scale is characterizing the bulk stratigraphy of the PLDs. The geologic relationships between the four packets of radar layers and the basal unit would be better constrained by radiometric age dates and/or exposure age dates of lithics contained in the PLD, Cavi, and Rupus units. These constraints would characterize the timespan and the largest temporal resolution contained within the PLDs.

Trough exposures, on the order of ~100s of meters, is the next scale. Identifying unconformities is a priority for understanding the completeness of the record contained in the PLDs because hiatuses in accumulation or periods of ablation could remove or fail to preserve some of the record, and measurements of stratigraphy better than current assets provide are necessary to identify all of the periods when materials were not accumulating. At this scale, the NPLD offers a more likely solution. Observations at the NPLD, whether in optical or radar wavelengths, are more easily integrated in part because of high internal scattering that hinders interpretation at the SPLD (Whitten and Campbell, 2018). Elucidating the evolution of the PLDs requires understanding changes in deposition rates by observing bedding geometry, thickness and unconformities to understand how deposition has changed through time.

Finally, it is important to study the current surface and upper meter of the PLDs at the sub-meter scale as described in Section 2.A.3. Understanding the fine-scale structures in the near-surface of the PLD is key to interpreting the deeper record because the finest layers made in the current epoch are likely to be created by the same processes that formed layers in the past.

We identified several key measurements that would address the above areas of needed knowledge and ranked them according to priority.

- Highest priority is to obtain an absolute age somewhere in the stratigraphy through cosmogenic/radiogenic nuclei abundance for a well-chosen location within the PLD. There are a variety of radiosotopic systems and methods available for age determination on the Earth (e.g. ^{14}C, ^{10}Be, K-Ar, ^{36}Cl, ^{3}He, ^{36}Ar, Ne). These methods may require finding and dating a lithic layer (e.g., impact or volcanic sediments, Fig. 8) or finding a clear climate signal in isotopologues of atmospheric gasses or water vapor. We discuss age dating in Section 2.A.5.

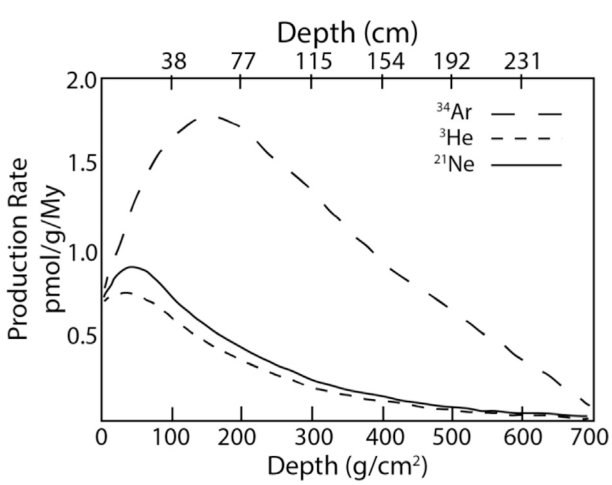

Fig. 8. Production of 34 Ar, 3He, and 22Ne with depth on Mars, modified from Farley et al. (2014).

- Intermediate priority was given to the search for patterns in vertical distribution of impurity fraction of isotopes (D/H, oxygen, and carbon being most important), and chemistry (iron, silica, aluminum, sulfur and chlorine) to match orbital history on the 100s of m depth scale. Annual layers are estimated to be on the microns to mm scale and obtaining that vertical resolution would assist in determining the smallest time resolution recorded in the PLD layers.
- Intermediate priority was also given to determining the completeness of the PLD by generating a catalogue of existing unconformities throughout the stack. Such unconformities, when mapped by radar and compared to climate models, have been useful in constraining ages (Putzig et al., 2009; Smith et al., 2016). Finer resolution mapping by improved resolution remote sensing would provide invaluable inputs to determining the PLD record.
- Low priority was given to the measurement of the crater size-frequency distribution (SFD) with depth to determine relative ages from vertical crater distribution. The vertical crater SFD would require higher resolution, and therefore higher power, radar than SHARAD to detect craters below the 7 km detected in initial surveys (Putzig et al., 2018). While absolute age results would still be crater production-function dependent, quantifying the crater size-frequency distribution with depth places relative age constraints on the PLDs.

2.1.5. Age dating the NPLD

In order to tie physical layers seen in radar to obliquity and climate cycles on Mars, age constraints must be placed on layered materials. In particular, obtaining at least one absolute age is critical for placing all layers above and below in some context of the greater system. Formation and exposure ages are obtained on Earth (and Mars, e.g. Farley et al., 2014) using radiogenic and cosmogenic nuclides. Briefly, cosmogenic nuclides are produced through any interaction of primary or secondary cosmic radiation with matter containing a range of target elements. Stable nuclides build up over time as a surface is exposed to cosmic rays. Radiogenic nuclides are daughter products of radioactive decay and build up on surfaces to the point of saturation, which refers to the state when the rate of production equals the rate of decay. When a surface is buried, the accumulation of cosmogenic and radiogenic nuclides slows down or stops entirely, depending on the nuclide (Fig. 8). The cosmogenic stable nuclides remain, while the radiogenic nuclides decay into stable daughters. The production rate of cosmogenic nuclides on Mars is estimated from meteorites, and can be used, along with a measurement of the abundance of these nuclides in a layer, to determine how long the material in the layer sat on the surface. The burial age of the material can then be determined by the difference between the abundance of cosmogenic nuclides in currently exposed surface materials vs. buried materials.

Cosmogenic and radiogenic dating techniques are widely used in studies of ice cores and glacial geomorphology on Earth, with ^{10}Be (half-life ~1.5 My), ^{26}Al (half-life ~700 ky), and ^{14}C (half-life ~5700 y) as the most frequently used dating systems (e.g., Fabel et al., 2002; Bond et al., 1993; Rinterknecht et al., 2006). For the most part, age dating is done on lithic material and volcanic ash entrained in ice, although in some cases trapped gases are analyzed (e.g., Buizert et al., 2014) with state-of-the-art noble gas mass spectrometers. However, the very large masses of ice (100s of kg) required for this technique to obtain sufficient material to analyze with high sensitivity, complicate applying this technique on Mars.

Cosmogenic and radiometric dating on Mars presents significant analytical challenges due to the amount of material necessary and the requirement (in most techniques) to have a robust mass estimate of material. A successful application of radiometric (K-Ar) and exposure age dating on Mars using cosmogenic ^{21}Ne, ^{3}He, and ^{38}Ar has been performed on Gale Crater mudstone (Farley et al., 2014) using the SAM instrument on Mars Science Laboratory (MSL). However, this work was done on martian regolith, where rocks with high concentrations of target elements (e.g., Mg, Ca, Al) ensure the presence of measurable abundances of cosmogenic nuclides.

Because the NPLD are mostly ice, achieving meaningful ages hinges on finding datable lithic material in the form of dust, volcanic ash, or impact ejecta that are accessible to robotic explorers. The estimated ~5 $\times 10^6$ years age of the NPLD also drives the requirement for extremely high precision measurements in order to achieve useful ages, with minimum age resolution on the order of 10^4–10^5 years. For comparison, the exposure age measurements achieved by SAM were 78 ± 30 million years (Farley et al., 2014), suggesting the need to improve precision by at least 2 orders of magnitude for meaningful measurements of the NPLD.

A mission to age-date the NPLD would require a highly selective and sensitive mass spectrometer similar in size, mass, and power to the SAM instrument on MSL. A range of mass spectrometry techniques to optimize exposure age dating using cosmogenic nuclides are currently in development to address the need for absolute age dating in planetary science. These techniques represent improvements in sensitivity, resolution, and selectivity over mass spectrometers currently used in planetary exploration. One promising technique in development is resonance ionization mass spectrometry (RIMS), which uses a laser or ion beam to remove neutral atoms from solids, then uses tuned lasers to excite electrons of a specific element and ionize it for measurement by mass spectrometer. This technique has been developed for the Rb–Sr geochronometer (Anderson et al., 2012, 2015) but could be applied to cosmogenic nuclides as well. In addition, recent developments using isotope dilution remove the need for obtaining a mass estimate, which should significantly reduce the magnitude of error (Farley et al., 2013). A precursor mission to confirm the presence and abundance of datable lithic material in the top 50 cm of the NPLD could inform efforts to refine these and other age dating techniques (e.g., Cohen et al., 2014) for later applications that access multiple layers.

2.2. Key properties and measurements

This section describes measurements to address our science priorities that can be made with existing and near future technology and the precision requirements associated with them.

2.2.1. Requirements for measurements of fluxes in the polar regions

Flux measurements will have to be performed at the surface in order to quantify fluxes that are directly relevant to deposition and ablation processes, and they should be supplemented by orbital measurements (as discussed above) in order to connect the surface measurements with the processes that govern the current global climate.

2.2.1.1. Measurement requirements. For fluxes, high frequency sampling of wind speed and direction in combination with temperature, pressure, and humidity are necessary. Particle flux should also be measured. To achieve this, wind measurements should have a precision of ten cm/s in three directions at a temporal resolution of ~20 Hz at least once per hour. Surface pressure measurements should provide long-term stability of 0.1 mbar with a precision of 0.02 mbar to be fruitful. Temperature measurements should fulfill a 0.5 K accuracy requirement. Characterization of heat and momentum fluxes in the lowermost polar atmosphere can develop from these measurements.

The accuracy requirement for humidity measurements is of order a few parts per million (ppm). Humidity measurements with a high temporal resolution (~20 Hz) in combination with wind measurements of the same resolution would allow the determination of water vapor transport through turbulent eddies. Alternatively, water vapor transport could be derived from similar frequency measurements of the water vapor gradient at 2–3 heights measured from a tall tower, the height of which would have to be determined.

Airborne dust and ice particles should be counted in aggregate to distinguish populations with respect to particle size to 1 μm and type, such as dust, CO_2 ice, and water ice. Together with hourly wind measurements, particulate measurements would enable the determination of dust and water ice particle transport through turbulent eddies. Depositional mass and dust to ices ratio are also required with microgram sensitivity. Furthermore, measurements of optical surface properties could supplement the characterization of environmental conditions and the interpretation of deposition and erosion measurements.

Five to six stations would be needed to accurately characterize these fluxes. Flux variations are expected to vary primarily with latitude and elevation so stations placed on the polar cap along one longitude at various latitudes, even equatorward of the polar cap margin, would capture the dependence on latitude and elevation.

2.2.1.2. Potential technologies. Wind speed and direction could be measured by a sonic anemometer or a wind lidar. The sonic anemometer can be set up to measure in three dimensions and would fulfill measurement requirements (Banfield and Dissly, 2005). This instrument could also measure temperature to an accuracy of ~0.2 K. Wind lidars are frequently used in ground-based applications on Earth; however, no wind lidar has been deployed on Mars. Hot wire or hot film anemometers, as deployed on Mars Pathfinder, Mars Science Laboratory, and InSight, do not have the measurement sensitivity to resolve turbulent eddies. Surface pressure can be measured by magnetic reluctance diaphragm sensors (Hess et al., 1977) or capacitive sensors (Gómez-Elvira et al., 2012a,b), which have extensive heritage for Mars surface missions.

For humidity measurements a laser hygrometer based on Tunable Diode Laser technology (TDL) provides high sensitivity at high repetition rates (Webster et al., 2004). Such an instrument has been deployed on the Mars Science Laboratory.

Measurements of dust and water ice mass flux could be achieved by aerosol optical detectors or nephelometers. Nephelometers measure particle densities that pass through a light beam and a light detector (e.g. a laser emitter and a photocell receiver) either in transmission or scattering geometry. They could also measure particle size distributions and optical properties. Deposition measurements could be made by a thermogravimeter or microbalance. These devices work with thermally stabilized piezoelectric transducers, whose frequency is proportional to the mass deposited on the sensor. They were proposed for the Martian Environmental Dust Systematic Analyser (MEDUSA) surface instrumentation package (Ventura, 2011). To determine the ratio of accumulation, heating the microbalance to sublimation temperatures would sublime deposited volatiles leaving just the dust. Measurement requirements and potential technologies for in-situ measurements are summarized in Table 1.

Simultaneous measurements from orbital assets should supplement *in-situ* measurements. Globally obtained vertical profiles of dust, water vapor, and water ice clouds would be necessary to connect the surface measurements with the processes that govern the current global climate. These kinds of vertical profiles have been provided, for example, by the MCS (Kleinböhl et al., 2009, 2017; McCleese et al., 2010) on MRO, and future instruments using lidar or sub mm spectroscopy can provide additional, critical information. Contributions to deposition and erosion processes could possibly be made using lidar or interferometric synthetic aperture radar (INSAR). However, it is likely that only the seasonal CO_2 frost could be measured in this way because other quantities would be beneath the detection limits of either instrument. It may be possible to support deposition and erosion studies by covering the polar ice with an artificial surface or a dye. Measuring changes in the optical properties of the surface over a season from a surface camera or from orbit would provide information on dust and ice accumulation. The dyed surface will likely change the surface roughness and radiative properties in comparison to an unmodified surface, so care is warranted in this approach.

2.2.2. Requirements for measurements of layer formation and properties

In the following section we consider measurements that would answer questions related to layer formation, age, composition, and stratification.

Table 1
Measurement requirements and potential technologies for in-situ flux measurements.

Measurement	Sensitivity requirement	Measurement frequency	# of stations	Potential technology
Wind (near surface)	few cm/s	20 Hz	5–6	Sonic anemometer
Water vapor/humidity	few ppm	20 Hz	5–6	Tunable Laser Spectrometer
Dust/water ice flux	aggregate of particles, μm radius	<1 Hz	5–6	Nephelometer
Dust/water ice accumulation	<1 μg	daily	5–6	Micro-balance (evaporation capabilities)

2.2.2.1. Layer formation. At the surface, determining the ratio of present-day accumulation of dust to H_2O to CO_2 is exceptionally important. A thermogravimeter with microgram accuracy can accumulate materials from snowfall and direct grain growth then measure to the microgram before heating the volatiles to the appropriate temperature for sublimation. These measurements will have to be made during polar winter, during accumulation of volatiles.

Measurements of surface albedo, texture, grain size (to 100 μm), grain density, and grain orientation should be made by reflectance spectroscopy in the infrared, a high-resolution imager, and nephelometry. Surface temperature can be measured with a thermal imager.

Understanding layer formation also requires access to the near subsurface, and drilling is the most appropriate method for reaching to 50 cm. Direct measurements of samples can either be done by lowering instruments into the bore hole or by transporting cuttings to lander deck instruments. Additionally, some techniques may permit thermal and electrical probes or fiber optic cables to be lowered in. We discuss implementation in later sections.

Drill telemetry can provide some of the required information. A 50 cm drill would offer rock/ice competency (in Pa) and density measurements within 20% error. Ideally, these measurements would be taken continuously, but discrete measurements would be sufficient.

Once a borehole is drilled, an optical imager could be lowered into the borehole in order to identify and count layers, layer thickness, and dip. Vertical resolution is a function of the device and the logging speed. Since the size of the smallest layer (or for that matter, what defines a layer) is unknown, we expect to need finer than 1 mm resolution in order to discern the thinnest, annual layers within the ice. After determining the most interesting layers, a microscope with ~30 μm resolution would record high-resolution imagery. Resistivity probes adequately adapted for Martian conditions and lowered within a borehole could be used to help correlate ground-penetrating radar (GPR) data with visible layers in the subsurface.

To measure grain size as a function of depth, techniques should have precision of 100 μm. The standard approach would be to observe thin sections from ice cores under polarized light. Within a borehole however, this quantity is difficult to measure. Sublimation occurs preferentially along grain boundaries (Obbard et al., 2006), so re-imaging the borehole at high resolutions 10s of days after it is created may allow grain boundaries to be visible. Alternatively, if the ice remains granular and porous within the uppermost meters then near-IR spectroscopy can be used to quantify grain sizes.

The distribution of impurities likely varies in the uppermost 50 cm because of active layer formation processes. To characterize impurity distribution, one option that provides nondestructive three-dimensional visualization of the internal features is miniaturized computerized tomography (microCT). This technology uses axial X-ray scans to obtain spatial resolution down to several microns. The technology uses a series of tomographic images taken at different sample angles to create a 3D reconstruction that can be analyzed with spatial resolution down to several microns. Numerous aspects of interest are in a vertical column: particle size and shape; volume concentration; pore size, shape, and distribution, discrimination of salts from Fe-rich sediment; and potentially relative atomic weight. It has been used extensively in the study of depositional processes in sedimentary rock (e.g. Falvard and Paris, 2017) and more recently in ice (Obbard et al., 2009; Iverson et al., 2017). MicroCT analysis has been able to differentiate ash layers from specific eruptions (Iverson et al., 2017).

2.2.2.2. Composition. On Earth, high precision measurements of impurities within the ice are conducted on drill cuttings or ice core sections. Analysis includes thin section stereology, ECM, meltwater analysis, ion and isotope chemistry, and microCT. However, this requires human intervention, and drilling and withdrawing cores robotically on Mars requires technology that does not exist. We discuss techniques to address this concern in later sections.

Trapped gases, such as CO_2, N_2, Ar, O_2, CO are in sufficient abundance to measure at a precision of 0.1% or greater, and minor constituents such as NO, Ne, HDO, Kr, and Xe require precision of 10–100 ppb. Other important volatile species like S, Cl, and CH_4 also require ppb precision. Bubble size and density should be measured to 10 μm.

Isotopic measurements should include D/H to a precision of 100/mil over the range of 100–9000 mil, $^{18}O/^{16}O$ at a precision of 3/mil, and $^{13}C/^{12}C$ at a precision of 5/mil. These measurements could be directly compared to isotopic measurements of the modern upper atmosphere by MAVEN or ancient hydrated minerals in Gale crater sediments and martian meteorites to inform models of long-term atmospheric escape. Concentrations of ^{10}Be are unknown, so determining if it is present in trace quantities will be valuable.

Composition and abundance of organics with a sensitivity of ppm to ppb is required.

Measurements should require determining the mineralogy of refractory minerals such as dust (an unconstrained assemblage of phases including nanophase ferric oxides and primary minerals) and primary mafic sediments to a precision of 1 wt%, distribution to 10 μm, and grain size for 1 μm particles and larger.

Similarly, S/Cl-rich salts (Morris et al., 2004; Yen et al., Hamilton et al., 2005; Yen et al., 2005) and perchlorate and sulfate salts (Horgan et al., 2009; Calvin et al., 2009; Massé et al., 2010, 2012) have been detected. Determining the mineralogy and elemental composition of soluble impurities such as these to a precision of 0.1 wt% is required.

2.2.2.3. Structure. Orbital measurements are better suited for large scale characterization than landed assets, and 10x higher resolution versions of existing instruments can provide more information than what we have presently. A stereoscopic optical imager with 10x improved resolution over HiRISE would identify finer layers and provide their geometries. An orbital sounding radar >100 MHz bandwidth would match present optical imagery. The higher resolution sounding radar with this bandwidth necessarily has a higher center frequency than existing assets, a trade that comes with a decrease in penetration depth unless compensated with a significant increase in transmit power. This trade increases cost and mass.

From the surface, geophysical techniques could be deployed as well. In order to resolve thin layers, a GPR with very high resolution and bandwidth (order 10 cm and GHz), that reaches >100 m penetration depth would provide exceptional quality checks on orbital measurements. Similarly, an advanced active source seismic system could resolve the layers and offer varying depth penetration depending on the separation of source and receiver.

Surface based optical imagery can aid here. In a borehole, an imager can look for layer tilt and of course measure layer thickness. Stereoscopic imagery from within the spiral troughs would have resolutions better than 10 cm and provide the unprecedented structure measurements. Equipment similar to gigapan cameras would be sufficient.

2.2.2.4. Borehole drilling. There are numerous technical challenges to overcome when drilling in cryogenic environments. We list some here:

Sampling resolution: Data acquisition with 0.5 mm spatial resolution would be difficult because of high data volumes and long duration measurements. Trading resolution for data rate is one possibility; however, the high value of the data warrants the best resolution possible.

Instrument integration and resources: Instrument miniaturization technology to fit within the borehole is required, and accommodation and further trade-offs must be considered.

Removal of drilled material*:* The smallest useful diameter of the borehole is likely to be around 5 cm. Thus, approximately 1000 cm^3 of material will need to be removed from the borehole. This material needs to be dumped close to the lander or transported by some means to the lander deck. Dumped material may alter or be mobilized by winds before measurements are made. Material moved from within the borehole requires technological advancements.

Borehole integrity: Continued drilling and measurements may be affected by material falling into the borehole or re-condensation of volatiles that sublimate during the drilling process and re-condense on the colder walls of the borehole.

Sediment layer: The mixing ratio of non-volatile material in individual layers is variable and may affect drilling operations. Newly exposed dust may be mobilized.

Diffusive loss of trapped gases: Sample handing may release the gases that were stored in the ice, losing important information in this investigation.

Other ice evolution: Assessment of how the ice evolves after it becomes exposed (in the borehole or the cuttings on the surface) is required. This involves volatilization or recrystallization.

Temperature Profile: Unique to deep borehole measurements, a vertical temperature profile could be measured, providing an additional insight into recent climate parameters such as the obliquity thermal wave and even the modern geothermal flux, however the drilling technique may affect temperature readings.

3. Mission concepts and approaches to measurements

Based on the science priorities and measurement requirements, we developed a multi-mission strategy that maximizes science return while maintaining a moderate budget. Some elements, like global wind speeds, and borehole measurements require a specific class of mission, while others can be distributed among classes for cost effectiveness.

The multi-mission strategy is to send an orbiter for global atmospheric and subsurface measurements, a static lander for polar reconnaissance of layers and near surface environments, a network of smallsats for distributed/network meteorology, and a fast, mobile platform or deep drill for narrow focus, rapid composition measurements. Each stage can be independent; however, science returns will be move valuable if the landed meteorology stations overlap in time with the orbiter. We detail these concepts in the next four sections.

3.1. Orbiter

An orbiter mission dedicated to the study of the martian polar regions has the potential to greatly advance our understanding of the present day forcings and fluxes in and out of the high latitudes and also help characterize fundamental properties of the PLD themselves.

Complete coverage of the planet at all local times would be ideal, but with a single orbiter trades-offs must be made. The main choices are between repeat coverage at one local time or greater time of day coverage. Each of these requires a different type of orbit; however, a hybrid scenario is conceivable, wherein an orbiter performs measurements at one local time for one Mars year and then changes local time for a second Mars year. Thus, time of day requirements can be accommodated without sacrificing polar coverage, such as CASSIS. Mars Odyssey has set the precedent for this option. Furthermore, starting with MRO's orbit would increase the baseline of current atmospheric observations for MCS and the Mars Color Imager (MARCI).

The science payload would be selected to fit within two broad themes: 1) Fluxes and Forcings, and 2) PLD Physical Properties. We note that several instruments have a very strong flight heritage and could potentially be proposed with slight technological improvements for big gains. See Table 2 for a list of instrument type and key measurement goals.

3.1.1. Fluxes and Forcings

Two instruments capable of meeting the highest priority of measuring global wind speeds for the first time: a microwave sounder and a LIDAR. Besides measuring wind speeds, either could provide profiles of temperature, water vapor and other tracers in the atmosphere.

A second instrument, such as an IR sounder inspired by MCS, would measure temperature, water vapor, dust, CO_2 and H_2O ice cloud profiles as well as surface temperature and emissivity. This would have the benefit of extending our current atmospheric measurements. Improvements over MCS to obtain 2-3x higher vertical resolution, better H_2O/aerosol discrimination, and better coverage closer to the surface are important.

A multi-wavelength visible/IR imager would measure surface frosts and discern water ice from CO_2. An instrument with heritage from MARCI that included more bands and higher spatial resolution would fill this role.

3.1.2. PLD physical properties

To measure fine layer sequences within the top 100s of meters of the PLD, we envision a radar sounding instrument with higher resolution than SHARAD and MARSIS. A P- or L-band sounder, with $>$100 MHz bandwidth could achieve vertical resolution better than 1 m. A synthetic aperture radar polarized (PolSAR) with interferometric capabilities (InSAR) on the order of 5 cm vertically would determine vertical changes of surface topography at the poles related to seasonal frost accumulation and mass wasting. This would supplement other instruments in characterizing energy and mass budgets of the PLD. This instrument, while being highly valuable for polar observations, would also provide measurements related to the global water ice and dust inventories.

Very high spatial resolution imagers (multi-wavelength visible, similar to HiRISE, and hyperspectral visible/near IR spectrometers, similar to CRISM) would have the potential to resolve finer layer structures within the stratigraphic record and constrain the composition of surface lags derived from internal dust/lithic layers. We note that to generate fundamentally new science information, the spatial resolution of these instruments would need to be an order of magnitude finer than current assets. Cost and sufficient signal to noise ratio are concerns.

A multipurpose scanning LIDAR instrument could provide valuable surface and atmosphere science. With 1 cm topography and 5 m shot points, it would detect surface changes and help characterize fluxes towards or out of the PLD. Multiple wavelengths could allow the discrimination of surface CO_2 and water ice and measure cloud heights within the polar night.

To fit within a Discovery or New Frontiers class mission, the high spatial resolution imagers and lidar would be the preferred descope options, in that order, leaving the meteorological and subsurface measurements.

Besides the obvious advantage of joining orbital meteorological measurements with landed meteorology (Sections 3.B and 3.C), hybrid missions between orbital and surface platforms would add value. Surface assets may be able to deploy surface calibration targets, reflectors, or radio beacons to improve the accuracy and precision for monitoring of changes. Impactor missions could gather data during descent and provide extremely high spatial resolution of surface and near surface properties. A surface instrument to disperse reflectors or a dye on the surface would allow an orbiter to monitor color and albedo changes as a means to determine the mass balance at specific locations. Color and albedo changes monitored from orbit could prove a means to determine the mass balance at multiple locations.

Table 2
Straw-man Orbiter Payload. Instruments are for an extremely capable orbiter with abundant power and data rates. The first de-scope options are the Microwave Nadir Sounder, Multi-wavelength visible imager, Near-IR pushbroom spectrometer and the LIDARS.

Instrument (in priority order)	Key Measurement	Performance Characteristics	Notes
Microwave or LIDAR Wind Profiler	Winds Speeds, Isotope tracking	3D wind speeds to 1 m/s	Critical for GCMs, never flown to Mars before
High-Resolution RADAR Sounder	MAP PLD layers and mid-latitude ice at high resolution	50 cm vertical resolution to 100 m	Complementary to SHARAD and MARSIS
PolSAR	Map extent of ground ice	<5 m horizontal resolution, polarimetry	Big power draw and data rates
InSAR	Temporal changes in topography, surface roughness	<1 cm vertical resolution	Big power draw and data rates
IR limb/Nadir Sounder	Vertical profiles of Temperature, Water Vapor, Aerosols	2x MCS + enhanced channels	Global atmospheric processes
Multi wavelength visible/IR imager	Measure surface frosts and discern H2O from CO2	Improved channels and resolution over MARCI	Two cameras for stereo observations of clouds
Multi-Wavelength LIDAR	High-resolution topography, CO2 and H2O composition, seasonal and interannual variability, cloud profiles	<1 cm vertical resolution, <5 m shot size, >4 wavelengths, atmospheric profiling	Works at night, measure seasonal accumulation, high precision orbit required
Multi-wavelength visible imager	Morphology, Albedo, Composition, Topography	1–10 cm	Resolve layers thinner than HiRISE, Context
Near-IR pushbroom spectrometer	Composition - H2O and CO2 Ices, Dust	Better than CRISM	Only works in sunlight

3.2. Static lander

Here we discuss a straw-man payload for a single static lander that has drilling capabilities, ice handling equipment and instruments, and a complete suite of atmospheric instruments (Table 3). We anticipate that a static lander is best suited as a reconnaissance mission designed to characterize the environment at the PLD, including the near subsurface.

This first delivery to the PLD surface should include instrumentation that is capable of addressing strategic knowledge gaps, including measuring all relevant atmospheric parameters and processes, observing surface changes and properties, and accessing the top 50 cm with full physical and chemical analysis (Table 3). The top 50 cm is chosen to reach layers that are predicted to no longer interact with the current atmosphere (Bramson et al., 2019). This mission could be of the NASA New Frontiers class and provide the groundwork for a future mobile mission designed to use the knowledge gained for rapid acquisition of stratigraphic measurements (see section 3.E).

Potential methods to reach 50 cm depth include thermal and mechanical drilling. Analysis may take place inside the borehole on the lander deck. Some instruments are too large to fit in a borehole, so a combination of techniques is considered. Because the 50 cm depth is very shallow, we concentrate on an approach that includes a mechanical drill, as opposed to a melt-probe. The main driver for using a mechanical drill, or a combined mechanical and melt drill, is the power savings. Cryogenic ice is 3-4x more conductive than warm ice, and as such, the melting approach would require a larger power supply (>80% of heat is lost into surrounding ice). There is the additional risk of finding layers with significant dust fraction that the drill could not penetrate, causing it to be stuck. That said, if thermal, or vaporizing drilling techniques could overcome these obstacles while maintaining high resolution, the benefit of not handling drill cuttings or risk of getting stuck outweigh a mechanical drill.

Table 3
Lander instrumentation. Drill (D); borehole logger (BL); lander deck (LD).

Type of measurement	Instrument	Heritage	Location	Comment
Optical	Pan-cam (multi-spec)	Many	D, BL, LD	
Optical	Microscope	Many	D, BL	
Environmental	Ground penetrating radar		LD	
Environmental	Met station	Many	LD	
Environmental	Ice and dust accumulation system		LD	Quartz-crystal microbalance?
Environmental	LIDAR	Phoenix	LD	
Analytical	Tunable laser spectrometer	MSL	LD	
Analytical	Mass spectrometer	Phoenix	LD	Connected via a vacuum pump and tubing to the mouth of the borehole
Analytical	Deep UV, Raman or VNIR (with fiberoptic lead)	Mars 2020	D, BL, LD	Fibre-fed from the borehole
Elemental	LIBS	MSL, Mars2020	D, BL, LD	Fibre-fed from the borehole
Ice structure	micro CT			Examine Core

3.2.1. In borehole analysis

Multiple options exist for in-borehole analysis. The first is to use the drill itself as an instrument. Drill-integrated instruments would help with the drilling process, reduce mechanical risks, and provide science data. The instruments and data include, material strength and density from drilling telemetry, density from ultrasonic velocity, a temperature sensor, and bulk electrical resistivity (required to detect "slush" formation and salt content) from resistivity sensor.

The second option is to modify the drill string to include instruments. This approach has numerous benefits, including *in situ* analysis of samples, but it also requires miniaturization technologies to be developed. Additionally, a drill string may not be capable of performing all of the science requirements, meaning that some material may have to be taken to the surface.

A third technique is to lower instruments into the borehole after the drill string is removed. This option has advantages over using the drill string because it reduces complexity of a complicated moving part; however, a trade is made because a separate articulating arm would be required, or the mechanical arm that operated the drill would have to detach from the drill and operate the borehole logger.

Instruments that could be built into the drill string or lowered separately include an optical camera system and/or a LED-driven VNIR spectrometer system, a microscope, a spectrometer (such as Ma_MISS on ExoMars, De Sanctis et al., 2017), a fine-scale electrical resistivity probe, a temperature sensor, and a laser (Table 3). The optical camera system should provide a wide field of view, such as a fish eye or acquire images by rotation. The microscope should have a short working distance and be able to reach micron resolutions. An optical camera, spectrometer, and the microscope will require some illumination. In addition, we foresee the inclusion of a laser in the borehole as a source for performing Laser Induced Breakdown Spectroscopy (LIBS) and deepUV/Raman (Bazalgette Courrèges-Lacoste et al., 2007)). The spectrometer would reside on the deck of the lander and be fed via fiber optic cable, while the laser would be integrated in the borehole logger. These instruments are ideal for measuring D/H or $^{18}O/^{16}O$, critical measurements for this mission. The alternative of keeping the laser on deck and using fiber optic cable to transmit the light increases risk of damage to the cable. Heritage of this type of instrument comes from the Mars 2020 Scanning Habitable Environments with Raman & Luminescence for Organics & Chemicals (SHERLOC) and SuperCam spectrometers.

Ice composition and ice grain size as well as the mineralogy of impurities could all be assessed rapidly via short-wave infrared reflectance spectroscopy (SWIR; 1.0–4.0 μm), which has been shown via orbital remote sensing to be highly sensitive to key phases in the PLD (references above) and has been successfully miniaturized for small applications.

Bulk chemistry of borehole walls or other solid samples could be assessed via X-ray fluorescence (XRF), as implemented in the Planetary Instrument for X-ray Lithochemistry (PIXL) instrument on Mars 2020, via alpha particle X-ray spectroscopy (APXS), as implemented on multiple Mars rovers, or via laser-induced breakdown spectroscopy (LIBS), as implemented in the MSL ChemCam and Mars 2020 SuperCam instruments. LIBS has been implemented with long fiber optics cables and may be more applicable to small diameter boreholes.

Additional instruments could also be packaged inside a borehole logger or drill string, but the extent of what can be included largely depends on several parameters. Increasing the diameter of the borehole would permit larger instruments to perform analysis, but this comes at an energy cost. Resistance to shock, vibrations and temperature are also concerns.

3.2.2. Sample analysis on the lander deck

The final option is to remove samples from the borehole for analysis on the lander deck. This may be done as a single core, drill cuttings, melting the cutting and transporting as a liquid, or volatilizing the sample. Each has advantages and disadvantages, and Technological advancements for robotic core handling would be required. Drill cuttings (also known as chips) of ~1 cm have to be transported to instruments many times, requiring a separate and durable sample handling system. Cuttings could be approximately 1 cm thick, and a pneumatic sample handling system integrated into the drilling apparatus could transport several cm^3 at a time to instruments on the lander deck (Fig. 9).

Instruments that we propose would remain on the lander deck to perform analysis include the high technology readiness level (TRL) pyrolysis gas chromatography-mass spectrometer with a laser desorption mass spectrometer (cf. the Mars Organic Molecule Analyser (MOMA) onboard the upcoming ExoMars Rover, Arevalo et al., 2015). These could be applied to detect and characterize organics, or potentially utilized for exposure age dating of sediments via cosmogenic nuclides. Tunable laser spectroscopy (TLS), as implemented on Curiosity, could provide information on the bulk and isotopic composition of major gases. Prior to destruction of the sample, a microCT should be employed to study the internal structure of the ice. Technology development for a flight ready microCT is necessary to complete these measurements.

3.2.3. Landing site selection

Landing site choice will be influenced by 1) safety to the mission and 2) completing our science requirements. If all sites are determined to be equally safe, then the optimal landing site will be one that maximizes science returns. Locations with greater surface-atmosphere activity (e.g. high mass balance and wind speeds) are preferred.

Another important consideration is subsurface layering, and we should avoid a location that has unique or local processes that do not represent the wider PLD. Compared to Earth, the PLDs are not as dynamic as the terrestrial ice sheets because layers are not significantly influenced by flow (Karlsson et al., 2011), and no melting is expected to occur at the surface or the base today. Radar surveys show continuous, sub-horizontal layers (Phillips et al., 2011) and small thickness variations (Nerozzi and Holt, 2017) across the lower ½ of the NPLD for more than 1000 km, so identifying an ice divide far from strong basal topography is not a priority.

3.3. Small-sat network

Numerous options are available for small-sat, short-lived missions that can perform rapid measurements while being scattered over the NPLD. In particular, the $Mars_{Drop}$ platform is of interest (Staehle et al., 2015). These units are approximately the size of a 6U cubesat and shaped like an ice-cream cone. The dome carries a parawing but no other EDL components, and descent is not guided. This is not critical for the types of investigations identified here, and distributing up to five landers along a longitude that reaches a band >10° latitude is entirely sufficient. Landing on a target more specific than the 1000 km diameter polar cap is not required. Once on the surface, several solar panels would deploy, revealing the payload (Fig. 10).

Because of their small size, $Mars_{Drop}$ spacecraft must contain targeted investigations. Multiple missions of this scale could be sent simultaneously to measure atmospheric properties, atmospheric constituents, or surface and subsurface properties. For the atmosphere, a sonic anemometer coupled with temperature, pressure, and humidity instruments would be a desirable component of a meteorological network scattered across the polar landscape. Sending a TLS to measure the atmospheric components could also be of high value. Finally, a package that is able to measure ice properties including electro-conductivity or

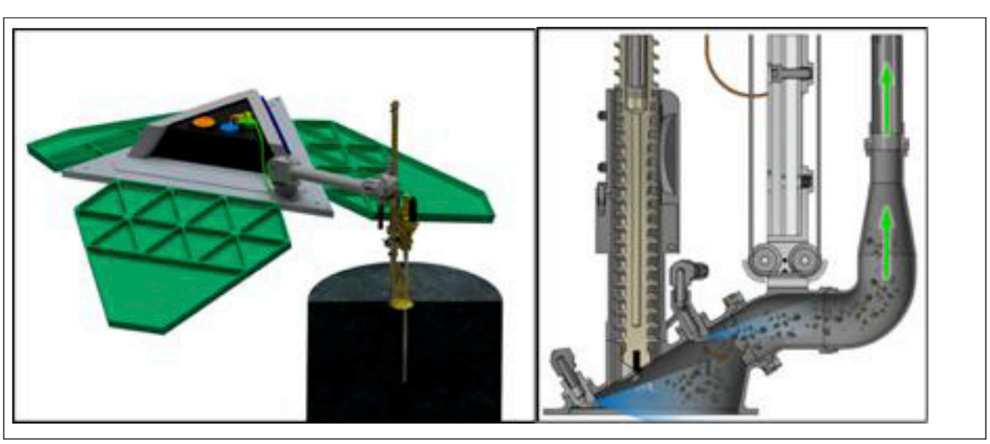

Figure 9. CAD concept of a lander asset using the Mars Exploration Rover (MER) Entry, Descent, and Landing (EDL) architecture. A) A drill arm extends past the landing hardware and mechanically drills ~50 cm into the subsurface using several small steps. B) Pneumatic hardware moves the drill cuttings to the lander deck where they can be analyzed by onboard instruments. Graphic courtesy of Honeybee Robotics.

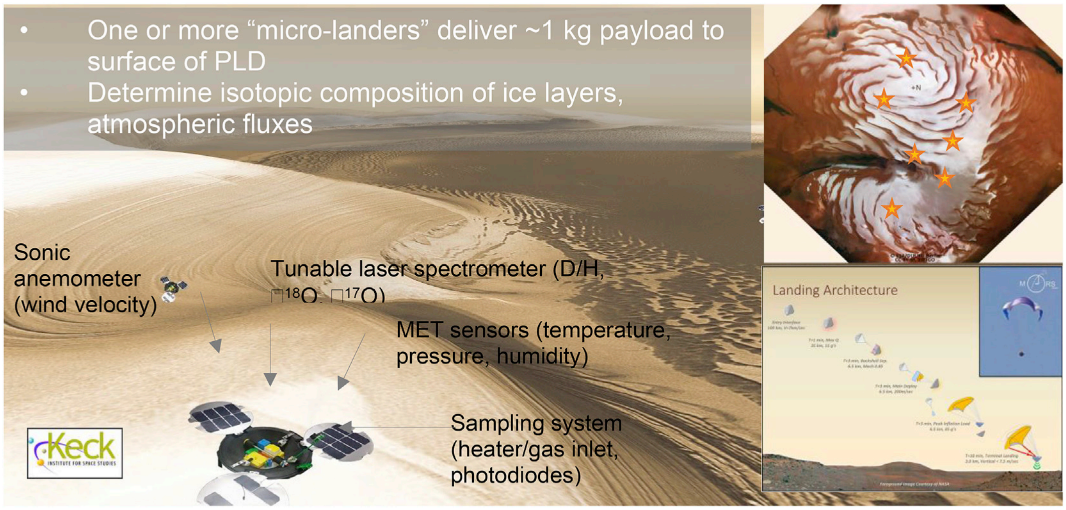

Fig. 10. Deployment of a network of small-sat MarsDrop spacecraft carrying either atmospheric or surface measurement instrumentation. Background from THEMIS draped over MOLA topography. Inset image from HRSC.

ground penetrating radar that could fit within the $Mars_{Drop}$ package would significantly contribute to the mission science.

3.4. Program architecture with two landed missions

Completion of the program to extract the climate record requires vertical sampling of ~500 m of stratigraphy, enough to obtain 1 Myr of climate history. This critical aspect is difficult to do economically while also performing all other science experiments desired. Therefore, we developed a two landed mission program that could complete all science objectives for the cost of two New Frontiers missions. This is a cost saving measure that has the additional benefits of being funded over multiple decades at the same time as reducing risk.

The first landed mission was a reconnaissance lander sent to measure all relevant atmospheric, surface, and subsurface properties and processes. The second landed mission could then concentrate on measuring only a narrow set of properties in a vertical section that directly tell of the climatic history. Repeating measurements related to ice and atmospheric properties is desirable but unnecessary, so the second landed mission could have a very small instrument set that acquired data very quickly. Because of the reduced number of investigations, this mission could potentially be completed in a single Mars spring and summer campaign rather than require capabilities to over winter. This mission, like the first, could fit into the New Frontiers program.

The two landed mission architecture has significant advantages over sending one extremely capable rover or deep drill capable of making every measurement that we identified as a priority. A single rover would certainly fall in the Flagship class and likely be the most capable robot ever sent to Mars with multiple technology programs for cold technology and miniaturization, increasing the total program cost by several times, reducing science return per dollar decreases. Further, in order to be cost conscious, science instruments would probably be de-scoped, leaving critical science goals unmet. Finally, the risk of a failure puts the entire program at jeopardy and ties NASA's hands for increased testing to guarantee success. This strategy bloats budgets with no compensatory gain. The complexity and cost of large, single missions and the risk of unmet science goals make them un-selectable.

Because the first landed mission would fall within the 2023–2032 decade, this second landed mission should come in the following decade, providing more time to develop platforms (Section 3.E) and spread the cost over many years.

3.5. Obtaining a long climate profile with extended vertical sampling

After the reconnaissance lander completes its task, we can complete the task of unlocking the climate record by accessing 500 m of vertical section in multiple ways that involve mobile or static landers. Three concepts are viable for follow-on landed missions. The first is a stationary platform with deep drilling capabilities, and the other two involve mobile platforms.

3.5.1. Viable second landed mission concepts

For a deep drill, instruments, would have to fit on the drill string to transmit information back to the surface via cables. Alternatives, such as extracting the drill and lowering instruments 500 m or handling 500 m of core without human intervention are technologically unfavorable.

Mechanical deep drilling technology for planetary missions is only at TRL 4 or 5 (AugoGopher2, WATSON), so sampling ~500 m of vertical stratigraphy would require an ambitious technology advancement program. Because of the reduced scientific payload (over a single landed mission), thermal drilling to complete the mission objectives becomes more viable, and thermal drilling has been proven at TRLs >5, reducing overall technological investments.

The first mobile platform option would involve sampling layers along a gently sloping trough wall. A rover that covers ten km of transect would access more than five hundred meters of outcrop. Local slopes, on 1–2 m thick layers could reach upwards of 15°, well within the capabilities of all modern rovers sent to Mars. Sliding is unlikely but could be mitigated with appropriate selection of traction. With a reduced payload and one high priority science objective, this rover would traverse more quickly than previous rovers, potentially in one Earth year.

The second option is a rappelling platform capable of descending a steep scarp near the margin of the PLD. The Axle-Rover is one possibility because it could land at a safe distance from the scarp and drive to it. Similar to the rover option, the limited instrument suite would mean very rapid measurements and quick mission completion.

Both mobile platforms would require abrading up to 10 cm of surface lag before making measurements. These technologies exist today, so little technological advancement is required.

The exact instruments on board these platforms cannot be decided until the first landed mission completes; however, we believe that some or all of the following suite may be necessary: a navigation camera that doubles for layer analysis; a chemistry suite encompassing wet geochemistry and a mass spectrometer; ground penetrating radar. Arm mounted instruments may include an optical imager, thermal and electrical conductivity, TLS, nephelometer, and micro-spectroscopy. *Any mission that accesses numerous layers should have instrumentation capable of finding an absolute age based on the first landed mission's reconnaissance*.

3.6. Surviving a polar night

Many of the desired measurements require surviving or operating in the polar night. At very high latitudes, a mission would have to survive extreme temperatures (~150 K) and endure approximately one earth year without solar energy. This is not achievable with current battery technology, so landed missions would be required to bring energy with them or create energy *in situ*. Options exist for both techniques, and each comes with risks.

One option would be to bring a radioisotope thermoelectric generator (RTG). The constant supply of power would enable measurements in the polar night, but the heat generated would likely alter the local environment and disturb the atmospheric and surface measurements. Mitigation would require some distance or insulation between the RTG and measurements.

Another option would be to bring chemical energy with the spacecraft. Materials may include fuel and oxygen for burning. This option requires extra mass and has risk associated with transporting volatiles. An advantage is that power could be on demand, so it would only be consumed when needed to charge batteries, or during heavy drill operation.

Creating energy *in situ* is currently an important topic of discussion. In lieu of bringing fuel, landers could use solar energy to create fuel such as hydrogen and oxygen through photolysis. On launch the tanks could begin empty, saving mass, and then be filled during the abundant energy period of summer. This requires splitting water molecules and storage and a technology development program.

Alternatively, recent research has found that CO_2 can react with lithium metal to produce large quantities of heat and electricity in the form of a battery (Xu et al., 2013; Qie et al., 2017). This choice would use the abundantly available CO_2 atmosphere to provide energy at significant cost savings over transporting energy to Mars. The technology has not yet been developed for planetary missions, so investments are required now to advance to high TRL by the next decade.

3.7. Planetary protection

Finally, a mission to locations with H_2O raises questions about forward contamination of biota to Mars. Under planetary protection definitions, the PLD are not considered special regions because they are not "a region within which terrestrial organisms are likely to propagate, or a region which is interpreted to have a high potential for the existence of extant Martian life forms." This is because of the long history without sufficient energy and temperatures to melt water. However, there is the possibility that an RTG could induce a special region by warming the ice to the melting point, and this possibility warrants consideration for mission planning.

That said, any forward contamination that takes hold in the induced special region is expected to be temporary. The PLD are many thousands of km away and geologically isolated from a location that could feature high enough water activity (e.g. subsurface near the equator), so terrestrial organisms are unlikely to survive transport through the irradiated atmosphere to find a habitat, possibly making this concern moot.

4. Conclusions

In this paper we outlined some of the overarching questions for Mars climate science going forward and have developed a roadmap for answering the questions with specific focus on the highest priority science. This plan uses experience gained from past and ongoing missions, as well as former proposal concepts, terrestrial field, and lab work.

The four most encompassing science question for unlocking the climate record are:

1 What are present and past fluxes of volatiles, dust, and other materials into and out of the polar regions?
2. How do orbital forcing and exchange with other reservoirs affect those fluxes?
3. What chemical and physical processes form and modify layers?
4. What is the timespan, completeness, and temporal resolution of the climate history recorded in the PLD?

Each question requires numerous measurements to address, and the climate record can only be fully extracted by answering all questions. That said, individual steps towards answering these questions would improve our knowledge of the state of Mars, and missions that address these core questions can be spread out over several decades. Thus, a program of multiple missions is the best route to understanding the climate record from the PLD.

Regarding the required missions, we carefully considered science return versus total cost and presented a multi-staged program that would address all of the highest priority science in a logical progression that eventually returns the climate record of Mars going back ~1 Myr.

The multi-mission program discussed here utilizes assets in orbit and on the surface. Of primary importance is new understanding of the present-day climate through enhanced and continued investigations of volatile and dust fluxes into and out of the polar regions and at the surface-atmosphere boundary. This is accomplished by making orbital measurements of dust, water vapor, and CO_2 transport globally through a suite of meteorological instruments. From orbit, subsurface measurements of volume, extent, purity, and porosity of volatile reservoirs is also critical to understanding the current climatic state. Simultaneously, if possible, a network of small, SIMPLEX level spacecraft distributed along a latitude band across $>10^{\circ}$ of latitude would provide the ground truth atmospheric observations necessary in order to calibrate the orbital measurements and observe surface-atmosphere interactions, including accumulation and ablation of volatiles at the poles.

Larger assets on the ground, in the form of a static reconnaissance lander followed by a mobile platform or deep drill, would then complete the task of extracting the climate record. First, a New Frontiers-class static lander would assess all qualities of the materials at the PLD surface and near (50 cm) subsurface in order to determine the most appropriate techniques for extracting the climate record, most likely by radio isotope measurements. Subsurface access would also enable us to determine how atmospheric properties and processes create and modify layers, including sintering and densification to the preserved layers.

We envision the final mission to be a highly focused mission that is designed to make very specific measurements through 500 m of vertical stratigraphy, accessing ~1 Myr of martian climate history. Three options include a rover to descend the shallow spiral troughs, a rappelling platform to descend the steep marginal scarps, or a deep drill. All would carry a narrow suite of instruments designed to only extract the information needed for obtaining the past climate, keeping this final mission within the New Frontiers Program.

The two-lander architecture reduces costs, complexity, and risk over sending a single extremely capable mission while being better adapted to accomplish the science goals. Further, the two landed-mission concept could be spread over multiple decades, leaving budget room for other missions. Multiple smaller missions have numerous advantages over single missions that are too large to fail.

As we discuss here, there are numerous reasons to investigate the polar regions of Mars. The modern climate state and the climate record are scientifically compelling targets, but the data required to advance our scientific understanding of ice and climate processes and history would also support the potential for human exploration by providing critical inputs to modern climate and available resources. In addition, the astrobiological potential of the polar ice also makes these compelling targets for future missions.

The polar layered deposits of Mars are the only other known place in the universe to host a detailed climate record on a terrestrial planet. Accessing that climate record is one of the most compelling objectives of NASA and a Holy Grail planetary science. By reading that climate record we can learn about the climate history of planets like our own throughout the universe. Our hypotheses are fully matured, and the time to begin this project is now.

Declaration of competing interest

We have no conflicts of interest.

Acknowledgements

We gratefully acknowledge the support of the Keck Institute of Space Studies who generously supported this meeting by hosting and facilitating all of our discussions. Work at the Jet Propulsion Laboratory, California Institute of Technology, is performed under contract with the National Aeronautics and Space Administration.

Appendix A. Supplementary data

Supplementary data related to this article can be found at https://doi.org/10.1016/j.pss.2020.104841.

References

Banks, M.E., Byrne, S., Galla, K., McEwen, A.S., Bray, V.J., Dundas, C.M., Fishbaugh, K.E., Herkenhoff, K.E., Murray, B.C., 2010. Crater population and resurfacing of the Martian north polar layered deposits. J. Geophys. Res. 115. E08006.
Fishbaugh, K.E., Hvidberg, C.S., Byrne, S., Russell, P.S., Herkenhoff, K.E., Winstrup, M., Kirk, R., 2010b. First high-resolution stratigraphic column of the Martian north polar layered deposits. Geophys. Res. Lett. 37 https://doi.org/10.1029/2009GL041642 n/a–n/a.
Grima, C., Kofman, W., Mouginot, J., Phillips, R.J., Hérique, A., Biccari, D., Seu, R., Cutigni, M., 2009. North polar deposits of Mars: extreme purity of the water ice. Geophys. Res. Lett. 36 https://doi.org/10.1029/2008GL036326 n/a–n/a.
Limaye, A.B.S., Aharonson, O., Perron, J.T., 2012. Detailed stratigraphy and bed thickness of the Mars north and south polar layered deposits. J. Geophys. Res. 117 https://doi.org/10.1029/2011JE003961 n/a–n/a.
Aharonson, O., Schorghofer, N., 2006. Subsurface ice on Mars with rough topography. J. Geophys. Res. 111, E11007. https://doi.org/10.1029/2005JE002636.
Albee, A., 2000. Report on the Loss of the Mars Polar Lander and Deep Space 2 Missions.
Anderson, F. Scott, et al., 2012. A laser desorption resonance ionization mass spectrometer for Rb-Sr geochronology: Sr isotope results. In: Aerospace Conference. IEEE. IEEE, 2012.
Anderson, F. Scott, et al., 2015. Rb-Sr resonance ionization geochronology of the Duluth Gabbro: a proof of concept for in situ dating on the Moon. Rapid Commun. Mass Spectrom. 29 (16), 1457–1464.
Appéré, T., Schmitt, B., Langevin, Y., Doute, S., Pommerol, A., Forget, F., Spiga, A., Gondet, B., Bibring, J.P., 2011. Winter and spring evolution of northern seasonal deposits on Mars from OMEGA on Mars Express. Journal of Geophysical Research-Planets 116. https://doi.org/10.1029/2010je003762.
Arevalo, R., Brinckerhoff, W., Ameromvan, F., Danell, R., Pinnick, V., Li, Xiang, Getty, S., Hovmand, L., Grubisic, A., Mahaffy, P., Goesmann, F., Steininger, H.. Design and demonstration of the Mars Organic Molecule Analyzer (MOMA) on the ExoMars 2018 rover. https://doi.org/10.1109/AERO.2015.7119073.
Arthern, R.J., Winebrenner, D.P., Waddington, E.D., 2000. Densification of water ice deposits on the residual north polar cap of Mars. Icarus 144, 367–381.
Banfield, D., Dissly, R., 2005. A Martian sonic anemometer. In: IEEE Aerospace Conference. https://doi.org/10.1109/AERO.2005.1559354.
Bapst, J., Byrne, S., Brown, A.J., 2018. On the icy edge at Louth and Korolev craters. Icarus, Mars Polar Science VI 308, 15–26. https://doi.org/10.1016/j.icarus.2017.10.004.
Bar-Cohen, Y., Zacny, K., 2009. Drilling in Extreme Environments Penetration and Sampling on Earth and Other Planets. John Wiley & Sons.
Barr, A.C., Milkovich, S.M., 2008. Ice grain size and the rheology of the martian polar deposits. Icarus 194 (2), 513–518.
Basu, S., Richardson, M.I., Wilson, R.J., 2004. Simulation of the martian dust cycle with the GFDL Mars GCM. J. Geophys. Res.: Plan 109 (E11).
Bazalgette Courrèges-Lacoste, G., Ahlers, B., Pérez, F.R., 2007. Combined Raman spectrometer/laser-induced breakdown spectrometer for the next ESA mission to Mars. Spectrochim. Acta Part A: Molecular and Biomolecular Spectroscopy, Seventh International Conference on Raman Spectroscopy Applied to the Earth and Planetary Sciences 68, 1023–1028. https://doi.org/10.1016/j.saa.2007.03.026.
Becerra, P., Byrne, S., Brown, A.J., 2015. Transient bright "halos"; on the south polar residual cap of Mars: implications for mass-balance. Icarus 251, 211–225. https://doi.org/10.1016/j.icarus.2014.04.050.
Becerra, P., Byrne, S., Sori, M.M., Sutton, S., Herkenhoff, K.E., 2016. Stratigraphy of the north polar layered deposits of Mars from high-resolution topography. J. Geophys. Res. Planets 1–27. https://doi.org/10.1002/(ISSN)2169-9100.
Becerra, P., Smith, I.B., Nunes, D.C., Sori, M.M., Thomas, N., Brouet, Y., Guallini, L., 2017a. Correlation of radar and visible data of Mars' north polar layered deposits. European Planetary Science Congress (EPSC abstract number EPSC2017-660).
Becerra, P., Sori, M.M., Byrne, S., 2017b. Signals of astronomical climate forcing in the exposure topography of the north polar layered deposits of Mars. Geophys. Res. Lett. 44, 62–70. https://doi.org/10.1002/2016GL071197.
Becerra, P., Sori, M.M., Thomas, N., Pommerol, A., Simioni, E., Sutton, S.S., Tulyakov, S., Cremonese, G., 2019. Timescales of the climate record in the south polar ice cap of Mars. Geophys. Res. Lett. 46, 7268–7277. https://doi.org/10.1029/2019GL083588.
Berman, D.C., Hartmann, W.K., 2002. Recent fluvial, volcanic, and tectonic activity on the Cerberus plains of Mars. Icarus 159 (1), 1–17.
Bibring, J.-P., Langevin, Y., Gendrin, A., Gondet, B., Poulet, F., Berthé, M., Soufflot, A., Arvidson, R., Mangold, N., Mustard, J., 2005. Mars surface diversity as revealed by the OMEGA/Mars Express observations. others Science 307, 1576–1581.
Bierson, C.J., Phillips, R.J., Smith, I.B., Wood, S.E., Putzig, N.E., Nunes, D., Byrne, S., 2016. Stratigraphy and evolution of the buried CO_2 deposit in the Martian south polar cap. Geophys. Res. Lett. 43 (9), 4172–4179. https://doi.org/10.1002/2016gl068457.
Bond, Gerard, et al., 1993. Correlations between climate records from North Atlantic sediments and Greenland ice. Nature 6442, 143–147, 365.
Böttger, H.M., Lewis, S.R., Read, P.L., Forget, F., 2005. The effects of the martian regolith on GCM water cycle simulations. Icarus 177 (1), 174–189.
Bramson, A.M., Byrne, S., Bapst, J., 2017. Preservation of midlatitude ice sheets on Mars. J. Geophys. Res.: Plan 122, 2250–2266. https://doi.org/10.1002/2017JE005357.
Bramson, A.M., Byrne, S., Bapst, J., Smith, I.B., McClintock, T., 2019. A migration model for the polar spiral troughs of Mars. J. Geophys. Res.: Plan 124, 1020–1043. https://doi.org/10.1029/2018JE005806.
Brothers, T.C., Holt, J.W., Spiga, A., 2015. Planum Boreum basal unit topography, Mars: irregularities and insights from SHARAD. J. Geophys. Res.: Plan 120, 1357–1375.
Brown, A.J., Piqueux, S., Titus, T.N., 2014. Interannual observations and quantification of summertime H2O ice deposition on the Martian CO2 ice south polar cap. Earth Planet Sci. Lett. 406, 102–109.
Brown, A.J., Calvin, W.M., Becerra, P., Byrne, S., 2016. Martian north polar cap summer water cycle. Icarus 277, 401–415. https://doi.org/10.1016/j.icarus.2016.05.007.
Buhler, P.B., Ingersoll, A.P., Ehlmann, B.L., Fassett, C.I., Head, J.W., 2017. How the martian residual south polar cap develops quasi-circular and heart-shaped pits, troughs, and moats. Icarus 286, 69–93. https://doi.org/10.1016/j.icarus.2017.01.012.
Buhler, P. B., Ingersoll, A.P., Piqueux, S., Ehlmann, B.E., Hayne, P.O. (in press). Coevolution of Mars's atmosphere and massive south polar CO2 ice deposit. Nature Astronomy. doi:10.1038/s41550-019-0976-8
Buizert, Christo, et al., 2014. Radiometric 81Kr dating identifies 120,000-year-old ice at Taylor Glacier, Antarctica. Proc. Natl. Acad. Sci. Unit. States Am. 111 (19), 6876–6881.
Byrne, S., 2004. Internal structure of the Martian south polar layered deposits. J. Geophys. Res. 109 https://doi.org/10.1029/2004JE002267, 43–20.
Byrne, S., 2009. The polar deposits of Mars. Annu. Rev. Earth Planet Sci. 37, 535–560. https://doi.org/10.1146/annurev.earth.031208.100101.
Byrne, S., Ingersoll, A.P., 2003. A sublimation model for martian south polar ice features. Science 299, 1051–1053. https://doi.org/10.1126/science.1080148.
Calvin, W.M., Roach, L.H., Seelos, F.P., Seelos, K.D., Green, R.O., Murchie, S.L., Mustard, J.F., 2009. Compact reconnaissance imaging spectrometer for Mars observations of northern martian latitudes in summer. Journal of Geophysical Research-Planets 114. https://doi.org/10.1029/2009je003348.
Calvin, W., et al., 2010. Planetary science decadal survey: Mars polar climate concepts. https://sites.nationalacademies.org/cs/groups/ssbsite/documents/webpage/ssb_059312.pdf.
Calvin, W.M., James, P.B., Cantor, B.A., Dixon, E.M., 2015. Interannual and seasonal changes in the north polar ice deposits of Mars: observations from MY 29-31 using MARCI. Icarus 251, 181–190. https://doi.org/10.1016/j.icarus.2014.08.026.
Carsey, F.D., et al., 2005a. NASA Vision Mission: Palmer Quest: Search for Life at the Bed of the Mars Polar Cap. California Institute of Technology, Jet Propulsion Laboratory.
Carsey, F.D., et al., 2005b. Palmer Quest: A Feasible Nuclear Fission "Vision Mission" to the Mars Polar Caps. LPSC #1844.
Chamberlain, M.A., Boynton, W.V., 2007. Response of Martian ground ice to orbit-induced climate change. J. Geophys. Res.: Plan 112. https://doi.org/10.1029/2006JE002801.
Christian, S., Holt, J.W., Byrne, S., Fishbaugh, K.E., 2013. Integrating radar stratigraphy with high resolution visible stratigraphy of the north polar layered deposits, Mars. Icarus 226, 1241–1251. https://doi.org/10.1016/j.icarus.2013.07.003.
Cohen, et al., 2014. The potassium-argon laser experiment (KArLE): in situ geochronology for Mars and beyond. In: 8th Int. Conf. On Mars. Pasadena. #1791.
Colaprete, A., Barnes, J.R., Haberle, R.M., Hollingsworth, J.L., Kieffer, H.H., Titus, T.N., 2005. Albedo of the south pole on Mars determined by topographic forcing of atmosphere dynamics. Nature 435, 184–188.
Colaprete, A., Barnes, J.R., Haberle, R.M., Montmessin, F., 2008. CO2 clouds, CAPE and convection on Mars: observations and general circulation modeling. Planet. Space Sci. 56 (2), 150–180.

Craddock, R.A., Greeley, R., 2009. Minimum estimates of the amount and timing of gases released into the martian atmosphere from volcanic eruptions. Icarus 204 (2), 512–526.
Cuffey, K., Paterson, W.S.B., 2010. The Physics of Glaciers, fourth ed. Academic Press, Elsevier, Hardcover, p. 704. 9780123694614.
Cutts, J.A., 1973. Nature and origin of layered deposits of the Martian polar regions. J. Geophys. Res. Planets 78, 4231–4249. https://doi.org/10.1029/JB078i020p04231.
Dahl-Jensen, D., Gundestrup, N.S., Miller, H., Watanabe, O., Johnsen, S.J., Steffensen, J.P., Clausen, H.B., Svensson, A., Larsen, L.B., 2002. The NorthGRIP deep drilling programme. Ann. Glaciol. 35, 1–4. https://doi.org/10.3189/172756402781817275.
De Sanctis, M.C., Altieri, F., Ammannito, E., Biondi, D., De Angelis, S., Meini, M., Mondello, G., Novi, S., Paolinetti, R., Soldani, M., Mugnuolo, R., Pirrotta, S., Vago, J.L., the Ma_Miss team, 2017. Ma_MISS on ExoMars: mineralogical characterization of the martian subsurface. Astrobiology 17, 612–620. https://doi.org/10.1089/ast.2016.1541.
Dequaire, J.M., Kahre, M.A., Haberle, R.M., Hollingsworth, J.L., 2014. July. Radiative effects of CO_2 ice clouds in the martian polar nights. In: Eighth International Conference on Mars, 1791, p. 1429.
Diniega, S., Smith, I.B., 2019. High-priority science questions identified at the Mars workshop on amazonian and present-day climate. Planet. Space Sci. https://doi.org/10.1016/j.pss.2019.104813.
Durand, G., 2006. Effect of impurities on grain growth in cold ice sheets, 10 colleagues J. Geophys. Res. 111. F01015.
Emmett, J.A., Murphy, J.R., 2018. Formation of the Martian Polar Layered Deposits: Quantifying Polar Water Ice and Dust Surface Deposition During Current and Past Orbital Epochs with the NASA Ames Mars GCM 2086, 4006.
Epica community members, 2004. Eight glacial cycles from an Antarctic ice core. Nature 429, 623–628. https://doi.org/10.1038/nature02599, 2004.
Fabel, Derek, et al., 2002. Landscape preservation under Fennoscandian ice sheets determined from in situ produced 10 Be and 26 Al. Earth Planet Sci. Lett. 201 (2), 397–406.
Falvard, S., Paris, R., 2017. X-ray tomography of tsunami deposits: Towards a new depositional model of tsunami deposits. Sedimentology 64, 453–477.
Fanale, F.P., Salvail, J.R., Zent, A.P., Postawko, S.E., 1986. Global distribution and migration of subsurface ice on mars. Icarus 67, 1–18. https://doi.org/10.1016/0019-1035(86)90170-3.
Farley, K.A., et al., 2013. A double-spike method for K–Ar measurement: a technique for high precision in situ dating on Mars and other planetary surfaces. Geochem. Cosmochim. Acta 110, 1–12.
Farley, K.A., et al., 2014. In situ radiometric and exposure age dating of the martian surface. Science 343 (6169), 1247166. https://doi.org/10.1126/science.1247166.
Feldman, W.C., Boynton, W.V., Jakosky, B.M., Mellon, M.T., 1993. Redistribution of subsurface neutrons caused by ground ice on Mars. J. Geophys. Res. Planets 98, 20855–20870. https://doi.org/10.1029/93JE02325.
Feldman, W.C., Boynton, W.V., Tokar, R.L., Prettyman, T.H., Gasnault, O., Squyres, S.W., Elphic, R.C., Lawrence, D.J., Lawson, S.L., Maurice, S., McKinney, G.W., Moore, K.R., Reedy, R.C., 2002. Global distribution of neutrons from Mars: results from Mars Odyssey. Science 297, 75–78. https://doi.org/10.1126/science.1073541.
Fishbaugh, K.E., Head, J.W., 2005. Origin and characteristics of the Mars north polar basal unit and implications for polar geologic history. Icarus 174, 444–474.
Fishbaugh, K.E., Hvidberg, C.S., 2006. Martian north polar layered deposits stratigraphy: implications for accumulation rates and flow. J. Geophys. Res. 111, 26819–26821. https://doi.org/10.1029/2005JE002571.
Fishbaugh, K.E., Byrne, S., Herkenhoff, K.E., Kirk, R.L., Fortezzo, C., Russell, P.S., McEwen, A., 2010a. Evaluating the meaning of "layer" in the martian north polar layered deposits and the impact on the climate connection. Icarus 205, 269–282. https://doi.org/10.1016/j.icarus.2009.04.011.
Fisher, D.A., 1993. If martian ice caps flow: ablation mechanisms and appearance. Icarus 105, 501–511.
Fisher, D.A., 2000. Internal layers in an "accublation" ice cap: a test for flow. Icarus 144, 289–294.
Fisher, D.A., 2007. Mars' water isotope (D/H) history in the strata of the North Polar Cap: inferences about the water cycle. Icarus 187, 430–441. https://doi.org/10.1016/j.icarus.2006.10.032.
Fisher, D.A., Hecht, M.H., Kounaves, S.P., Catling, D.C., 2010. A perchlorate brine lubricated deformable bed facilitating flow of the north polar cap of Mars: possible mechanism for water table recharging. J. Geophys. Res.: Plan 115.
Forget, F., Pollack, J.B., 1996. Thermal infrared observations of the condensing Martian polar caps: CO2 ice temperatures and radiative budget. J. Geophys. Res.: Plan 101, 16865–16879.
Forget, F., Hourdin, F., Fournier, R., Hourdin, C., Talagrand, O., Collins, M., Lewis, S.R., Read, P.L., Huot, J.P., 1999. Improved general circulation models of the Martian atmosphere from the surface to above 80 km. J. Geophys. Res.: Plan 104 (E10), 24155–24175.
Forget, F., Haberle, R.M., Montmessin, F., Levrard, B., Head, J.W., 2006. Formation of glaciers on Mars by atmospheric precipitation at high obliquity. Science 311 (5759), 368–371.
Foss II, F.J., Putzig, N.E., Campbell, B.A., Phillips, R.J., 2017. 3-D imaging of Mars' polar ice caps using orbital radar data. Lead. Edge 36 (1), 43–57. https://doi.org/10.1190/tle36010043.1.
Gómez-Elvira, J., et al., 2012a. REMS: the environmental sensor suite for the Mars Science Laboratory rover. Space Sci. Rev. 170, 583–640.
Gómez-Elvira, J., Armiens, C., Castañer, L., Domínguez, M., Genzer, M., Gómez, F., Haberle, R., Harri, A.-M., Jiménez, V., Kahanpää, H., Kowalski, L., Lepinette, A., Martín, J., Martínez-Frías, J., McEwan, I., Mora, L., Moreno, J., Navarro, S., de Pablo, M.A., Peinado, V., Peña, A., Polkko, J., Ramos, M., Renno, N.O., Ricart, J., Richardson, M., Rodríguez-Manfredi, J., Romeral, J., Sebastián, E., Serrano, J., de la Torre Juárez, M., Torres, J., Torrero, F., Urquí, R., Vázquez, L., Velasco, T., Verdasca, J., Zorzano, M.-P., Martín-Torres, J., 2012b. REMS: the environmental sensor suite for the Mars science laboratory rover. Space Sci. Rev. 170, 583–640. https://doi.org/10.1007/s11214-012-9921-1.
Gow, A.J., 1969. On the rates of growth of grains and crystals in South Polar firn. J. Glaciol. 8, 241–252.
Grimm, R.E., Harrison, K.P., Stillman, D.E., Kirchoff, M.R., 2017. On the secular retention of ground water and ice on Mars. J. Geophys. Res.: Plan 122, 94–109. https://doi.org/10.1002/2016JE005132.
Guo, X., Lawson, W.G., Richardson, M.I., Toigo, A., 2009. Fitting the viking lander surface pressure cycle with a Mars general circulation model. J. Geophys. Res.: Plan 114 (E7).
Haberle, R., Kahre, M.A., 2010. Detecting secular climate change on Mars. MARS 5, 68–75. https://doi.org/10.1555/mars.2010.0003.
Haberle, R.M., Murphy, J.R., Schaeffer, J., 2003. Orbital change experiments with a Mars general circulation model. Icarus 161 (1), 66–89.
Haberle, R.M., Forget, F., Colaprete, A., Schaeffer, J., Boynton, W.V., Kelly, N.J., Chamberlain, M.A., 2008. The effect of ground ice on the Martian seasonal CO_2 cycle. Planet. Space Sci. 56 (2), 251–255.
Haberle, R.M., Kahre, M.A., Schaeffer, J.R., Montmessin, F., Phillips, R.J., 2012. A Cloud Greenhouse Effect on Mars: Significant Climate Change in the Recent Past.
Haberle, R.M., de la Torre Juárez, M., Kahre, M.A., Kass, D.M., Barnes, J.R., Hollingsworth, J.L., Harri, A.-M., Kahanpää, H., 2018. Detection of northern hemisphere transient eddies at Gale crater Mars. Icarus 307, 150–160. https://doi.org/10.1016/j.icarus.2018.02.013.
Hamilton, V.E., Mcsween, H.Y., Hapke, B., 2005. Mineralogy of Martian Atmospheric Dust Inferred from Thermal Infrared Spectra of Aerosols, 110, p. 12006. https://doi.org/10.1029/2005JE002501.
Hayne, P.O., Paige, D.A., Heavens, N.G., Mars Climate Sounder Science Team, 2014. The role of snowfall in forming the seasonal ice caps of Mars: models and constraints from the Mars Climate Sounder. Icarus 231, 122–130.
Head, J.W., Mustard, J.F., Kreslavsky, M.A., Milliken, R.E., Marchant, D.R., 2003. Recent ice ages on Mars. Nature 426, 797–802.
Hecht, M.H., 2006. CHRONOS: a journey through martian history. In: Fourth International Mars Polar Science Conference. #8096.
Hecht, M.H., Saunders, R.S., 2003. Cryoscout: a descent through the Mars polar cap. In: Third International Mars Polar Science Conference. #8078.
Hecht, M.H., Kounaves, S.P., Quinn, R.C., West, S.J., Young, S.M.M., Ming, D.W., Catling, D.C., Clark, B.C., Boynton, W.V., Hoffman, J., DeFlores, L.P., Gospodinova, K., Kapit, J., Smith, P.H., 2009. Detection of perchlorate and the soluble chemistry of martian soil at the Phoenix lander site. Science 325, 64–67. https://doi.org/10.1126/science.1172466.
Herkenhoff, K., Plaut, J.G., 2000. Surface ages and resurfacing rates of the polar layered deposits on Mars. Icarus 144, 243–253. https://doi.org/10.1006/icar.1999.6287.
Herkenhoff, K.E., Byrne, S., Russell, P.S., Fishbaugh, K.E., McEwen, A.S., 2007. Meter-scale morphology of the north polar region of Mars. Science 317, 1711–1715. https://doi.org/10.1126/science.1143544.
Herny, C., Massé, M., Bourgeois, O., Carpy, S., Le Mouélic, S., Appéré, T., Smith, I.B., Spiga, A., Rodriguez, S., 2014. Sedimentation waves on the martian north polar cap: analogy with megadunes in Antarctica. Earth Planet Sci. Lett. 403, 56–66. https://doi.org/10.1016/j.epsl.2014.06.033.
Herr, K.C., Pimentel, G.C., 1969. Infrared absorptions near 3 microns recorded over the polar cap of Mars. Science 166, 496–499.
Hess, S.L., Henry, R.M., Leovy, C.B., Ryan, J.A., Tillman, J.E., 1977. Meteorological results from the surface of Mars: viking 1 and 2. J. Geophys. Res. 82, 4559–4574.
Holt, J.W., Fishbaugh, K.E., Byrne, S., Christian, S., Tanaka, K., Russell, P.S., Herkenhoff, K.E., Safaeinili, A., Putzig, N.E., Phillips, R.J., 2010. The construction of chasma Boreale on Mars. Nature 465, 446–449. https://doi.org/10.1038/nature09050.
Horgan, B., Bell, J.F., 2012. Widespread weathered glass on the surface of Mars. Geology 40 (5), 391–394. https://doi.org/10.1130/g32755.1.
Horgan, B.H., Bell, J.F., Noe Dobrea, E.Z., Cloutis, E.A., Bailey, D.T., Craig, M.A., Roach, L.H., Mustard, J.F., 2009. Distribution of hydrated minerals in the north polar region of Mars. J. Geophys. Res.: Plan 114 (E1), 27. https://doi.org/10.1029/2008JE003187.
Horgan, B.H.N., Cloutis, E.A., Mann, P., Bell, J.F., 2014. Near-infrared spectra of ferrous mineral mixtures and methods for their identification in planetary surface spectra. Icarus 234, 132–154. https://doi.org/10.1016/j.icarus.2014.02.031.
Howard, A.D., 2000. The role of eolian processes in forming surface features of the martian polar layered deposits. Icarus 144, 267–288.
Howard, A.D., Cutts, J.A., Blasius, K.R., 1982. Stratigraphic relationships within Martian polar cap deposits. Icarus 50, 161–215.
Hvidberg, C.S., Fishbaugh, K.E., Winstrup, M., Svensson, A., Byrne, S., Herkenhoff, K.E., 2012. Reading the climate record of the martian polar layered deposits. Icarus 221, 405–419. https://doi.org/10.1016/j.icarus.2012.08.009.
Hvidberg, C.S., Svensson, A., Buchardt, S.L., 2013. Ice dynamcis of the Greenland ice sheet. In: Scott, Elias, Mock, Cary (Eds.), Encyclopedia of Quaternary Science, second ed.
Icesag, 2019. Report from the Ice and Climate Evolution Science Analysis Group (ICE-SAG), Mars Exploration Program Analysis Group Topical Analysis Reports.
Iverson, N.A., Lieb-Lappen, R., Dunbar, N.W., Obbard, R., Kim, E., Golden, E., 2017. The first physical evidence of subglacial volcanism under the West Antarctic Ice Sheet. Sci. Rep. 7, 11457. https://doi.org/10.1038/s41598-017-11515-3.

Jakosky, B.M., 2012. Mars atmospheric D/H: Consistent with polar volatile theory? J. Geophys. Res.: Solid Earth 1475–1480. https://doi.org/10.1029/JB095iB02p01475@10.1002/(ISSN)2169-9356.POLMARS1.
Jakosky, B., Phillips, R., 2001. Mars' volatile and climate history. Nature 412, 237–244. https://doi.org/10.1038/35084184.
James, P.B., North, G.R., 1982. The seasonal CO2 cycle on Mars: an application of an energy balance climate model. J. Geophys. Res.: Solid Earth 87, 10271–10283. https://doi.org/10.1029/JB087iB12p10271.
Kadish, S.J., Head, J.W., Barlow, N.G., Marchant, D.R., 2008. Martian pedestal craters: marginal sublimation pits implicate a climate-related formation mechanism. Geophys. Res. Lett. 35 (16).
Kahre, M.A., Murphy, J.R., Haberle, R.M., 2006. Modeling the Martian dust cycle and surface dust reservoirs with the NASA Ames general circulation model. J. Geophys. Res.: Plan 111 (E6).
Kahre, M.A., Haberle, R.M., Hollingsworth, J.L., Wilson, R.J., 2018. Could a significant water ice cloud greenhouse have persisted throughout much of the amazonian? LPI Contrib. 4032, 2086.
Karlsson, N.B., Holt, J.W., Hindmarsh, R.C.A., 2011. Testing for flow in the north polar layered deposits of Mars using radar stratigraphy and a simple 3D ice-flow model. Geophys. Res. Lett. 38. L24204.
Karlsson, N.B., Schmidt, L.S., Hvidberg, C.S., 2015. Volume of Martian mid-latitude glaciers from radar observations and ice-flow modelling. Geophys. Res. Lett. 42, 2627–2633. https://doi.org/10.1002/2015GL063219.
Kieffer, H.H., 1990. H_2O grain size and the amount of dust in Mars' residual north polar CAP. J. Geophys. Res. 95, 1481–1493.
Kleinböhl, A., Schofield, J.T., Kass, D.M., Abdou, W.A., Backus, C.R., Sen, B., Shirley, J.H., Lawson, W.G., Richardson, M.I., Taylor, F.W., Teanby, N.A., McCleese, D.J., 2009. Mars Climate Sounder limb profile retrieval of atmospheric temperature, pressure, dust and water ice opacity. J. Geophys. Res. 114 https://doi.org/10.1029/2009JE003358. E10006.
Kleinböhl, A., Friedson, A.J., Schofield, J.T., 2017. Two-dimensional radiative transfer for the retrieval of limb emission measurements in the martian atmosphere. J. Quant. Spectrosc. Radiat. Transfer 187, 511–522.
Koenig, L.S., Ivanoff, A., Alexander, P.M., MacGregor, J.A., Fettweis, X., Panzer, B., Paden, J.D., Forster, R.R., Das, I., McConnell, J.R., Tedesco, M., Leuschen, C., Gogineni, P., 2016. Annual Greenland accumulation rates (2009–2012) from airborne snow radar. Cryosphere 10, 1739–1752. https://doi.org/10.5194/tc-10-1739-2016.
Koutnik, M., Byrne, S., Murray, B., 2002. south polar layered deposits of Mars: the cratering record. J. Geophys. Res. Planets 107, 5100–5101. https://doi.org/10.1029/2001JE001805.
Lalich, D.E., Holt, J.W., 2017. New Martian climate constraints from radar reflectivity within the north polar layered deposits. Geophys. Res. Lett. 44, 657–664. https://doi.org/10.1002/2016GL071323.
Lambert, F., Delmonte, B., Petit, J.R., Bigler, M., Kaufmann, P.R., Hutterli, M.A., Stocker, T.F., Ruth, U., Steffensen, J.P., Maggi, V., 2008. Dust-climate couplings over the past 800,000 years from the EPICA Dome C ice core. Nature 452, 616–619. https://doi.org/10.1038/nature06763.
Landis, M.E., Byrne, S., Daubar, I.J., Herkenhoff, K.E., Dundas, C.M., 2016. A revised surface age for the north polar layered deposits of Mars. Geophys. Res. Lett. 43, 3060–3068. https://doi.org/10.1002/2016GL068434.
Langevin, Y., Poulet, F., Bibring, J.P., Gondet, B., 2005. Summer evolution of the north polar cap of Mars as observed by OMEGA/Mars express. Science 307 (5715), 1581–1584.
Langevin, Y., Bibring, J.-P., Montmessin, F., Forget, F., Vincendon, M., Douté, S., Poulet, F., Gondet, B., 2007. Observations of the south seasonal cap of Mars during recession in 2004–2006 by the OMEGA visible/near-infrared imaging spectrometer on board Mars Express. J. Geophys. Res.: Plan 112. https://doi.org/10.1029/2006JE002841.
Laskar, J., Levrard, B., Mustard, J.F., 2002. Orbital forcing of the martian polar layered deposits. Nature 419, 375–377. https://doi.org/10.1038/nature01066.
Laskar, J., Correia, A.C.M., Gastineau, M., Joutel, F., Levrard, B., Robutel, P., 2004. Long term evolution and chaotic diffusion of the insolation quantities of Mars. Icarus 170, 343–364. https://doi.org/10.1016/j.icarus.2004.04.005.
Leighton, R.R., Murray, B.C., 1966. Behavior of carbon dioxide and other volatiles on Mars. Science 153, 136–144.
Levrard, B., Forget, F., Montmessin, F., Laskar, J., 2007. Recent formation and evolution of northern Martian polar layered deposits as inferred from a Global Climate Model. J. Geophys. Res. 112 https://doi.org/10.1029/2006JE002772, 5044–18.
Levy, J.S., Fassett, C.I., Head, J.W., Schwartz, C., Watters, J.L., 2014. Sequestered glacial ice contribution to the global Martian water budget: geometric constraints on the volume of remnant, midlatitude debris-covered glaciers. J. Geophys. Res. Planets 119. https://doi.org/10.1002/2014JE004685, 2014JE004685.
Listowski, C., Määttänen, A., Riipinen, I., Montmessin, F., Lefèvre, F., 2013. Near-pure vapor condensation in the Martian atmosphere: CO_2 ice crystal growth. J. Geophys. Res.: Plan 118 (10), 2153–2171.
MacGregor, J.A., Fahnestock, M.A., Catania, G.A., Paden, J.D., Gogineni, S.P., Young, S.K., Rybarski, S.C., Mabrey, A.N., Wagman, B.M., Morlighem, M., 2015. Radiostratigraphy and age structure of the Greenland ice sheet. J. Geophys. Res. Earth Surf. 120 https://doi.org/10.1002/2014JF003215.
Madeleine, J.B., Forget, F., Head, J.W., Levrard, B., Montmessin, F., Millour, E., 2009. Amazonian northern mid-latitude glaciation on Mars: a proposed climate scenario. Icarus 203 (2), 390–405.
Madeleine, J.B., Head, J.W., Forget, F., Navarro, T., Millour, E., Spiga, A., Colaïtis, A., Määttänen, A., Montmessin, F., Dickson, J.L., 2014. Recent ice ages on Mars: the role of radiatively active clouds and cloud microphysics. Geophys. Res. Lett. 41 (14), 4873–4879.
Malin, M.C., Edgett, K.S., 2001. Mars global surveyor Mars orbiter camera: interplanetary cruise through primary mission. J. Geophys. Res.: Plan 106. https://doi.org/10.1029/2000JE001455, 23429–23570.
Malin, M.C., Carr, M.H., Danielson, G.E., Davies, M.E., Hartmann, W.K., Ingersoll, A.P., James, P.B., Masursky, H., McEwen, A.S., Soderblom, L.A., Thomas, P., Veverka, J., Caplinger, M.A., Ravine, M.A., Soulanille, T.A., Warren, J.L., 1998. Early views of the martian surface from the Mars orbiter camera of Mars global surveyor. Science 279, 1681–1685. https://doi.org/10.1126/science.279.5357.1681.
Manning, C.V., McKay, C.P., Zahnle, K.J., 2006. Thick and thin models of the evolution of carbon dioxide on Mars. Icarus 180, 38–59.
Manning, C.V., Bierson, C., Putzig, N.E., McKay, C.P., 2019. The formation and stability of buried polar CO2 deposits on Mars. Icarus 317, 509–517. https://doi.org/10.1016/j.icarus.2018.07.021.
Massé, M., Bourgeois, O., Le Mouélic, S., Verpoorter, C., Le Deit, L., Bibring, J.-P., 2010. Martian polar and circum-polar sulfate-bearing deposits: sublimation tills derived from the North Polar Cap. Icarus 209 (2), 434–451. https://doi.org/10.1016/j.icarus.2010.04.017.
Massé, M., Bourgeois, O., Le Mouélic, S., Verpoorter, C., Spiga, A., Le Deit, L., 2012. Wide distribution and glacial origin of polar gypsum on Mars. Earth Planet Sci. Lett. 317–318, 44–55. https://doi.org/10.1016/j.epsl.2011.11.035.
McCleese, D.J., Heavens, N.G., Schofield, J.T., Abdou, W.A., Bandfield, J.L., Calcutt, S.B., Irwin, P.G.J., Kass, D.M., Kleinböhl, A., Lewis, S.R., Paige, D.A., Read, P.L., Richardson, M.I., Shirley, J.H., Taylor, F.W., Teanby, N., Zurek, R.W., 2010. Structure and dynamics of the Martian lower and middle atmosphere as observed by the Mars Climate Sounder: seasonal variations in zonal mean temperature, dust, and water ice aerosols. J. Geophys. Res. 115, E12016. https://doi.org/10.1029/2010JE003677.
McEwen, A.S., Eliason, E.M., Bergstrom, J.W., Bridges, N.T., Hansen, C.J., Delamere, W.A., Grant, J.A., Gulick, V.C., Herkenhoff, K.E., Keszthelyi, L., Kirk, R.L., Mellon, M.T., Squyres, S.W., Thomas, N., Weitz, C.M., 2007. Mars reconnaissance Orbiter's high resolution imaging science experiment (HiRISE). J. Geophys. Res. 112 https://doi.org/10.1029/2005JE002605, 8048–40.
Medley, B., Joughin, I., Smith, B.E., Das, S.B., Steig, E.J., Conway, H., Gogineni, S., Lewis, C., Criscitiello, A.S., McConnell, J.R., van den Broeke, M.R., Lenaerts, J.T.M., Bromwich, D.H., Nicolas, J.P., Leuschen, C., 2014. Constraining the recent mass balance of Pine Island and Thwaites glaciers, West Antarctica, with airborne observations of snow accumulation. Cryosphere 8, 1375–1392. https://doi.org/10.5194/tc-8-1375-2014.
Mellon, M.T., Boynton, W.V., Feldman, W.C., Arvidson, R.E., Titus, T.N., Bandfield, J.L., Putzig, N.E., Sizemore, H.G., 2008. A prelanding assessment of the ice table depth and ground ice characteristics in Martian permafrost at the Phoenix landing site. J. Geophys. Res.: Plan 113. https://doi.org/10.1029/2007JE003067@10.1002/(ISSN)2169-9100.PHOENIX1.
Mellon, M.T., Jakosky, B.M., 1993. Geographic variations in the thermal and diffusive stability of ground ice on Mars. J. Geophys. Res. Planets 3345–3364. https://doi.org/10.1029/92JE02355@10.1002/(ISSN)2169-9100.MARTSURF1.
Milkovich, S.M., Head, J.W., 2005. North polar cap of Mars: polar layered deposit characterization and identification of a fundamental climate signal. J. Geophys. Res. 110 https://doi.org/10.1029/2004JE002349, 140–21.
Milkovich, S.M., Plaut, J.J., 2008. Martian south polar layered deposit stratigraphy and implications for accumulation history. J. Geophys. Res. 113 https://doi.org/10.1029/2007JE002987 s.
Milkovich, S.M., Plaut, J.J., Safaeinili, A., Picardi, G., Seu, R., Phillips, R.J., 2009. Stratigraphy of Promethei Lingula, south polar layered deposits, Mars, in radar and imaging data sets. J. Geophys. Res. 114, 420–421. https://doi.org/10.1029/2008JE003162.
Mischna, M.A., Richardson, M.I., 2005. A reanalysis of water abundances in the Martian atmosphere at high obliquity. Geophys. Res. Lett. 32 https://doi.org/10.1029/2004GL021865.
Mischna, M.A., Richardson, M.I., Wilson, R.J., McCleese, D.J., 2003. On the orbital forcing of Martian water and CO_2 cycles: a general circulation model study with simplified volatile schemes. J. Geophys. Res.: Plan 108 (E6).
Montabone, L., Forget, F., Millour, E., Wilson, R.J., Lewis, S.R., Cantor, B., Kass, D., Kleinböhl, A., Lemmon, M.T., Smith, M.D., others, 2015. Eight-year climatology of dust optical depth on Mars. Icarus 251, 65–95.
Montmessin, F., Rannou, P., Cabane, M., 2002. New insights into Martian dust distribution and water-ice cloud microphysics. J. Geophys. Res.: Plan 107 (E6).
Montmessin, F., Forget, F., Rannou, P., Cabane, M., Haberle, R.M., 2004. Origin and role of water ice clouds in the Martian water cycle as inferred from a general circulation model. J. Geophys. Res.: Plan 109 (E10).
Montmessin, F., Fouchet, T., Forget, F., 2005. Modeling the annual cycle of HDO in the Martian atmosphere. J. Geophys. Res. 110, E03006. https://doi.org/10.1029/2004JE002357.
Montmessin, F., Haberle, R.M., Forget, F., Langevin, Y., Clancy, R.T., Bibring, J.P., 2007. On the origin of perennial water ice at the south pole of Mars: a precession-controlled mechanism? J. Geophys. Res.: Plan 112 (E8).
Morris, R.V., et al., 2004. Mineralogy at gusev crater from the mössbauer spectrometer on the spirit rover. Science 305 (5), 833–837. https://doi.org/10.1126/science.1100020.
Murchie, S., Arvidson, R., Bedini, P., Beisser, K., Bibring, J.-P., Bishop, J., Boldt, J., Cavender, P., Choo, T., Clancy, R.T., Darlington, E.H., Des Marais, D., Espiritu, R., Fort, D., Green, R., Guinness, E., Hayes, J., Hash, C., Heffernan, K., Hemmler, J., Heyler, G., Humm, D., Hutcheson, J., Izenberg, N., Lee, R., Lees, J., Lohr, D., Malaret, E., Martin, T., McGovern, J.A., McGuire, P., Morris, R., Mustard, J., Pelkey, S., Rhodes, E., Robinson, M., Roush, T., Schaefer, E., Seagrave, G., Seelos, F.,

Silverglate, P., Slavney, S., Smith, M., Shyong, W.-J., Strohbehn, K., Taylor, H., Thompson, P., Tossman, B., Wirzburger, M., Wolff, M., 2007. Compact reconnaissance imaging spectrometer for Mars (CRISM) on Mars reconnaissance orbiter (MRO). J. Geophys. Res. 112 https://doi.org/10.1029/2006JE002682. E05S03.
Murray, B.C., Soderblom, L.A., Cutts, J.A., Sharp, R.P., Milton, D.J., Leighton, R.B., 1972. Geological framework of the south polar region of Mars. Icarus 17, 328–345.
National Research Council, 2011. Vision and Voyages for PLanetary Science in the Decade 2013-2022. The National Academies Press, Washington, DC.
Navarro, T., Madeleine, J.B., Forget, F., Spiga, A., Millour, E., Montmessin, F., Määttänen, A., 2014. Global climate modeling of the Martian water cycle with improved microphysics and radiatively active water ice clouds. J. Geophys. Res.: Plan 119 (7), 1479–1495.
Navarro, T., Forget, F., Millour, E., Greybush, S.J., Kalnay, E., Miyoshi, T., 2017. The challenge of atmospheric data assimilation on Mars. Earth and Space Science 4, 690–722. https://doi.org/10.1002/2017EA000274.
Neem Community members, 2013. Eemian interglacial reconstructed from a Greenland folded ice core. Nature 493, 489–494. https://doi.org/10.1038/nature11789.
Nerozzi, S., W Holt, J., 2017. Earliest accumulation history of the north polar layered deposits, Mars from SHARAD. Icarus. https://doi.org/10.1016/j.icarus.2017.05.027.
Nerozzi, S., Holt, J.W., 2019. Buried ice and sand caps at the north Pole of Mars: revealing a record of climate change in the cavi unit with SHARAD. Geophys. Res. Lett. 46, 7278–7286. https://doi.org/10.1029/2019GL082114.
Newman, C.E., Lewis, S.R., Read, P.L., Forget, F., 2002. Modeling the Martian dust cycle 2. Multiannual radiatively active dust transport simulations. J. Geophys. Res.: Plan 107 (E12), 7-1.
Newman, C.E., Lewis, S.R., Read, P.L., 2005. The atmospheric circulation and dust activity in different orbital epochs on Mars. Icarus 174 (1), 135–160.
Nunes, D.C., Phillips, R.J., 2006. Radar subsurface mapping of the polar layered deposits on Mars. J. Geophys. Res. 111 https://doi.org/10.1029/2005JE002609, 5042–16.
Nunes, D.C., Smrekar, S.E., Fisher, B., Plaut, J.J., Holt, J.W., Head, J.W., Kadish, S.J., Phillips, R.J., 2011. Shallow Radar (SHARAD), pedestal craters, and the lost Martian layers: initial assessments. J. Geophys. Res.: Plan 116. https://doi.org/10.1029/2010JE003690.
Obbard, R., Baker, I., Sieg, K., 2006. Using electron backscatter diffraction patterns to examine recrystallization in polar ice sheets. J. Glaciol. 52, 546–557.
Obbard, R.W., Troderman, G., Baker, I., 2009. Imaging brine and air inclusions in sea ice using micro-X-ray computed tomography. J. Glaciol. 55, 1113–1115. https://doi.org/10.3189/002214309790794814.
Orosei, R., Lauro, S.E., Pettinelli, E., Cicchetti, A., Coradini, M., Cosciotti, B., Paolo, F.D., Flamini, E., Mattei, E., Pajola, M., Soldovieri, F., Cartacci, M., Cassenti, F., Frigeri, A., Giuppi, S., Martufi, R., Masdea, A., Mitri, G., Nenna, C., Noschese, R., Restano, M., Seu, R., 2018. Radar evidence of subglacial liquid water on Mars. Science 361, 490–493. https://doi.org/10.1126/science.aar7268.
Paige, D.A., Bachman, J.E., Keegan, K.D., 1994. Thermal and albedo mapping of the polar regions of Mars using Viking thermal mapper observations: 1. North polar region. J. Geophys. Res. Planets 99, 25959–25991. https://doi.org/10.1029/93JE03428.
Pathare, A.V., Paige, D.A., 2005. The effects of martian orbital variations upon the sublimation and relaxation of north polar troughs and scarps. Icarus 174, 419–443.
Perron, J.T., Huybers, P., 2009. Is there an orbital signal in the polar layered deposits on Mars? Geology 37, 155–158. https://doi.org/10.1130/G25143A.1.
Phillips, R.J., Zuber, M.T., Smrekar, S.E., Mellon, M.T., Head, J.W., Tanaka, K.L., Putzig, N.E., Milkovich, S.M., Campbell, B.A., Plaut, J.J., Safaeinili, A., Seu, R., Biccari, D., Carter, L.M., Picardi, G., Orosei, R., Mohit, P.S., Heggy, E., Zurek, R.W., Egan, A.F., Giacomoni, E., Russo, F., Cutigni, M., Pettinelli, E., Holt, J.W., Leuschen, C.J., Marinangeli, L., 2008. Mars north polar deposits: stratigraphy, age, and geodynamical response. Science 320, 1182–1185. https://doi.org/10.1126/science.1157546.
Phillips, R.J., Davis, B.J., Tanaka, K.L., Byrne, S., Mellon, M.T., Putzig, N.E., Haberle, R.M., Kahre, M.A., Campbell, B.A., Carter, L.M., Smith, I.B., Holt, J.W., Smrekar, S.E., Nunes, D.C., Plaut, J.J., Egan, A.F., Titus, T.N., Seu, R., 2011. Massive CO_2 ice deposits sequestered in the south polar layered deposits of Mars. Science 332, 838. https://doi.org/10.1126/science.1203091.
Picardi, G., Biccari, D., Seu, R., Marinangeli, L., Johnson, W.T.K., Jordan, R.L., Plaut, J., Safaenili, A., Gurnett, D.A., Ori, G.G., Orosei, R., Calabrese, D., Zampolini, E., 2004. Performance and surface scattering models for the Mars advanced radar for subsurface and Ionosphere sounding (MARSIS). Planet. Space Sci. 52, 149–156. https://doi.org/10.1016/j.pss.2003.08.020.
Piqueux, S., Kleinbohl, A., Hayne, P.O., Kass, D.M., Schofield, J.T., McCleese, D.J., 2015. Variability of the Martian seasonal CO_2 cap extent over eight Mars Years. Icarus 251, 164–180.
Plaut, J.J., Picardi, G., Safaeinili, A., Ivanov, A.B., Milkovich, S.M., Cicchetti, A., Kofman, W., Mouginot, J., Farrell, W.M., Phillips, R.J., Clifford, S.M., Frigeri, A., Orosei, R., Federico, C., Williams, I.P., Gurnett, D.A., Nielsen, E., Hagfors, T., Heggy, E., Stofan, E.R., Plettemeier, D., Watters, T.R., Leuschen, C.J., Edenhofer, P., 2007. Subsurface radar sounding of the south polar layered deposits of Mars. Science 316, 92–95. https://doi.org/10.1126/science.1139672.
Putzig, N.E., Mellon, M.T., 2007. Apparent thermal inertia and the surface heterogeneity of Mars. Icarus 191, 68–94. https://doi.org/10.1016/j.icarus.2007.05.013.
Putzig, N.E., Phillips, R.J., Campbell, B.A., Holt, J.W., Plaut, J.J., Carter, L.M., Egan, A.F., Bernardini, F., Safaeinili, A., Seu, R., 2009. Subsurface structure of planum Boreum from Mars reconnaissance orbiter shallow radar soundings. Icarus 204, 443–457. https://doi.org/10.1016/j.icarus.2009.07.034.
Putzig, N.E., Mellon, M.T., Herkenhoff, K.E., Phillips, R.J., Davis, B.J., Ewer, K.J., Bowers, L.M., 2014. Thermal behavior and ice-table depth within the north polar erg of Mars. Icarus, Third Planetary Dunes Systems 230, 64–76. https://doi.org/10.1016/j.icarus.2013.07.010.
Putzig, N.E., Smith, I.B., Perry, M.R., Foss, F.J., Campbell, B.A., Phillips, R.J., Seu, R., 2018. Three-dimensional radar imaging of structures and craters in the Martian polar caps. Icarus, Mars Polar Science VI 308, 138–147. https://doi.org/10.1016/j.icarus.2017.09.023.
Qie, L., Lin, Y., Connell, J.W., Xu, J., Dai, L., 2017. Highly rechargeable lithium-CO2 batteries with a Boron-and nitrogen-codoped holey-graphene cathode. Angew. Chem. Int. Ed. 56, 6970–6974.
Rinterknecht, V.R., et al., 2006. The last deglaciation of the southeastern sector of the Scandinavian Ice Sheet. Science311 5766, 1449–1452.
Ruddiman, W.F., 2006. Orbital changes and climate. In: Quaternary Science Reviews, 25, pp. 3092–3112.
Russell, P., Thomas, N., Byrne, S., Herkenhoff, K., Fishbaugh, K., Bridges, N., Okubo, C., Milazzo, M., Daubar, I., Hansen, C., McEwen, A., 2008. Seasonally active frost-dust avalanches on a north polar scarp of Mars captured by HiRISE. Geophys. Res. Lett. 35 https://doi.org/10.1029/2008GL035790.
Schenk, P.M., Moore, J.M., 2000. Stereo topography of the south polar region of Mars: volatile inventory and Mars Polar Lander landing site. J. Geophys. Res. 105, 24529–24546. https://doi.org/10.1029/1999JE001054.
Schmidt, F., et al., 2009. Albedo control of seasonal south polar cap recession on Mars. Icarus 200, 374–394.
Seu, R., Phillips, R.J., Biccari, D., Orosei, R., Masdea, A., Picardi, G., Safaeinili, A., Campbell, B.A., Plaut, J.J., Marinangeli, L., Smrekar, S.E., Nunes, D.C., 2007. SHARAD sounding radar on the Mars reconnaissance orbiter. J. Geophys. Res. 112 https://doi.org/10.1029/2006JE002745, 8073–18.
Simonsen, S.B., Stenseng, L., Adalgeirsdottir, G., Fausto, R.S., Hvidberg, C.S., 2013. Assessing a multi-layered dynamic firn-compaction model for Greenland with ASIRAS radar measurements. J. Glaciol. 59 (215), 545–558. https://doi.org/10.3189/2013JoG12J158.
Sinha, P., Horgan, B., Seelos, F., 2019. Dateable volcanic and impact sediments within the north polar layered deposits on Mars. In: Lunar and Planetary Science Conference. Abst, p. 2132.
Smith, M.D., 2008. Spacecraft observations of the Martian atmosphere. Annu. Rev. Earth Planet Sci. 36, 191–219. https://doi.org/10.1146/annurev.earth.36.031207.124335.
Smith, I.B., Holt, J.W., 2010. Onset and migration of spiral troughs on Mars revealed by orbital radar, 465 (7297), 450–453. https://doi.org/10.1038/nature09049.
Smith, I.B., Holt, J.W., 2015. Spiral trough diversity on the north pole of Mars, as seen by Shallow Radar (SHARAD). J. Geophys. Res. Planets 120, 362–387. https://doi.org/10.1002/2014JE004720.
Smith, D.E., Zuber, M.T., Frey, H.V., Garvin, J.B., Head, J.W., Muhleman, D.O., Pettengill, G.H., Phillips, R.J., Solomon, S.C., Zwally, H.J., 2001. Mars orbiter laser altimeter: experiment summary after the first year of global mapping of Mars (paper 2000JE001364). J. Geophys. Res.-All Series- 106, 23–689.
Smith, I.B., Holt, J.W., Spiga, A., Howard, A.D., Parker, G., 2013. The spiral troughs of Mars as cyclic steps. J. Geophys. Res.: Plan 118, 1835–1857. https://doi.org/10.1002/jgre.2014.
Smith, I.B., Putzig, N.E., Holt, J.W., Phillips, R.J., 2016. An ice age recorded in the polar deposits of Mars. Science 352, 1075–1078. https://doi.org/10.1126/science.aad6968.
Smith, I.B., Diniega, S., Beaty, D.W., Thorsteinsson, T., Becerra, P., Bramson, A.M., Clifford, S.M., Hvidberg, C.S., Portyankina, G., Piqueux, S., Spiga, A., Titus, T.N., 2018. 6th international conference on Mars polar science and exploration: conference summary and five top questions. Icarus. https://doi.org/10.1016/j.icarus.2017.06.027.
Sori, M.M., Byrne, S., Hamilton, C.W., Landis, M.E., 2016. Viscous flow rates of icy topography on the north polar layered deposits of Mars. Geophys. Res. Lett. 43, 541–549.
Sowers, T., Bender, M., Raynaud, D., Korotkevich, I.S., 1992. Delta N-15 of N2 in air trapped in polar ice - a tracer of gas transport in the firn and a possible constraint on ice age-gas age differences. J. Geophys. Res. 97, 15.
Staehle, Robert L., November 1976. “Mars Polar Ice Sample Return Mission” (Part 1). Spaceflight.
Staehle, Robert L., Fine, Sheryl A., Roberts, Andrew, Schulenberg, Carl R., Skinner, David L., 1977. “Mars Polar Ice Sample Return Mission” (Parts 2 & 3), *Spaceflight*. November & December.
Staehle, Robert L., Spangelo, Sara, Eby, Matthew, Lane, Marc S., Aaron, Kim M., Bhartia, Rohit, Boland, Justin S., Christiansen, Lance E., Forouhar, Siamak, de la Torre Juarez, Manuel, Paige, David A., Trawny, Nikolas, Webster, Chris R., Rebecca, M., Williams, E., 2015 August 13. Multiplying Mars lander Opportunities with MARSDROP microlanders. In: Conference Paper for: AIAA/USU Small Satellite Conference SSC15-XI-3. https://doi.org/10.13140/RG.2.1.3599.1127. Logan, Utah.
Steffensen, J.P., Andersen, K.K., Bigler, M., Clausen, H.B., Dahl-Jensen, D., Fischer, H., Goto-Azuma, K., Hansson, M., Johnsen, S.J., Jouzel, J., Masson-Delmotte, V., Popp, T., Rasmussen, S.O., Röthlisberger, R., Ruth, U., Stauffer, B., Siggaard-Andersen, M.-L., Sveinbjörnsdóttir, A.E., Svensson, A., White, J.W.C., 2008. High resolution Greenland ice core data show abrupt climate change happens in few years. Science 321 (5889), 680–684. https://doi.org/10.1126/science.1157707.
Svensson, A., Nielsen, S.W., Kipfstuhl, S., Johnsen, S.J., Steffensen, J.P., Bigler, M., Ruth, U., Röthlisberger, R., 2005. Visual stratigraphy of the north Greenland ice core project (NorthGRIP) ice core during the last glacial period. J. Geophys. Res. 110 https://doi.org/10.1029/2004JD005134. D02108.
Svensson, A., Andersen, K.K., Bigler, M., Clausen, H.B., Dahl-Jensen, D., Davies, S.M., Johnsen, S.J., Muscheler, R., Parrenin, F., Rasmussen, S.O., Röthlisberger, R., Seierstad, I., Steffensen, J.P., Vinther, B.M., 2008. A 60 000 year Greenland stratigraphic ice core chronology. Clim. Past 4, 47–57.

Tanaka, K.L., 2005. Geology and insolation-driven climatic history of Amazonian north polar materials on Mars. Nature 437, 991–994. https://doi.org/10.1038/nature04065.

Tanaka, K.L., Fortezzo, C.M., 2012. Geologic map of the north polar region of Mars. U.S. Geological Survey Scientific Investigations Map 3177 ([WWW Document]).

Tanaka, K.L., Kolb, E.J., Fortezzo, C., 2007. Recent Advances in the Stratigraphy of the Polar Regions of Mars, vols. 1–4.

Tanaka, K., Rodriguez, J., Skinner jr., J., Bourke, M., Fortezzo, C., Herkenhoff, K., Kolb, E., Okubo, C., 2008. North polar region of Mars: advances in stratigraphy, structure, and erosional modification. Icarus 196, 318–358. https://doi.org/10.1016/j.icarus.2008.01.021.

Tedesco, M., Doherty, S., Fettweis, X., Alexander, P., Jeyaratnam, J., Stroeve, J., 2016. The Darkening of the Greenland Ice Sheet: Trends, Drivers, and Projections, 10, pp. 477–496. https://doi.org/10.7916/D8ZG84R3, 1981–2100.

Thomas, P.C., James, P.B., Calvin, W.M., Haberle, R., Malin, M.C., 2009. Residual south polar cap of Mars: stratigraphy, history, and implications of recent changes. Icarus 203 (2), 352–375. https://doi.org/10.1016/j.icarus.2009.05.014.

Thomas, P.C., Calvin, W., Cantor, B., Haberle, R., James, P.B., Lee, S.W., 2016. Mass balance of Mars' residual south polar cap from CTX images and other data. Icarus 268, 118–130. https://doi.org/10.1016/j.icarus.2015.12.038.

Tillman, J.E., Johnson, N.C., Guttorp, P., Percival, D.B., 1993. The martian annual atmospheric pressure cycle: years without great dust storms. J. Geophys. Res.: Plan 98, 10963–10971, 1991–2012.

Titus, T.N., Kieffer, H.H., Christensen, P.R., 2003. Exposed water ice discovered near the south Pole of Mars. Science 299, 1048–1051. https://doi.org/10.1126/science.1080497.

Toon, O.B., Pollack, J.B., Ward, W., Burns, J.A., Bilski, K., 1980. The astronomical theory of climatic change on Mars. Icarus 44 (3), 552–607.

Vaughan, D.G., Comiso, J.C., Allison, I., Carrasco, J., Kaser, G., Kwok, R., Mote, P., Murray, T., Paul, F., Ren, J., Rignot, E., Solomina, O., Steffen, K., Zhang, T., 2013. Observations: cryosphere. In: Stocker, T.F., Qin, D., Plattner, G.-K., Tignor, M., Allen, S.K., Boschung, J., Nauels, A., Xia, Y., Bex, V., Midgley, P.M. (Eds.), Climate Change 2013: the Physical Science Basis. Contribution of Working Group I to the Fifth Assessment Report of the Intergovernmental Panel on Climate Change. Cambridge University Press, Cambridge, United Kingdom and New York, NY, USA.

Ventura, S., 2011. The MEDUSA and MicroMED Experiments for the ExoMars Space Programme to Perform in Situ Analysis of Martian Dust. https://doi.org/10.6092/UNINA/FEDOA/8541 [WWW Document].

Veres, D., Bazin, L., Landais, A., Toyé Mahamadou Kele, H., Lemieux-Dudon, B., Parrenin, F., Martinerie, P., Blayo, E., Blunier, T., Capron, E., 2013. The Antarctic ice core chronology (AICC2012): an optimized multi-parameter and multi-site dating approach for the last 120 thousand years. Clim. Past 9, 1733–1748.

Villanueva, G.L., Mumma, M.J., Novak, R.E., Käufl, H.U., Hartogh, P., Encrenaz, T., Tokunaga, A., Khayat, A., Smith, M.D., 2015. Strong water isotopic anomalies in the martian atmosphere: probing current and ancient reservoirs. Science 348, 218–221, 6231.

Vos, E., Aharonson, O., Schorghofer, N., 2019. Dynamic and isotopic evolution of ice reservoirs on Mars. Icarus 324, 1–7. https://doi.org/10.1016/j.icarus.2019.01.018.

Webster, C.R., Flesch, G.J., Mansour, K., Haberle, R., Bauman, J., 2004. Mars laser hygrometer. Appl. Optic. 43, 4436–4445.

Whiteway, J.A., Komguem, L., Dickinson, C., Cook, C., Illnicki, M., Seabrook, J., Popovici, V., Duck, T.J., Davy, R., Taylor, P.A., Pathak, J., Fisher, D., Carswell, A.I., Daly, M., Hipkin, V., Zent, A.P., Hecht, M.H., Wood, S.E., Tamppari, L.K., Renno, N., Moores, J.E., Lemmon, M.T., Daerden, F., Smith, P.H., 2009. Mars water-ice clouds and precipitation. Science 325, 68–70.

Whitten, J.L., Campbell, B.A., 2018. Lateral continuity of layering in the Mars south polar layered deposits from SHARAD sounding data. J. Geophys. Res.: Plan 123, 1541–1554. https://doi.org/10.1029/2018JE005578.

Winebrenner, D.P., Koutnik, M.R., Waddington, E.D., Pathare, A.V., Murray, B.C., Byrne, S., Bamber, J.L., 2008. Evidence for ice flow prior to trough formation in the martian north polar layered deposits. Icarus 195, 90–105.

Winter, A., Steinhage, D., Arnold, E.J., Blankenship, D.D., Cavitte, M.G.P., Corr, H.F.J., Paden, J.D., Urbini, S., Young, D.A., Eisen, O., 2017. Comparison of measurements from different radio-echo sounding systems and synchronization with the ice core at Dome C, Antarctica. Cryosphere 11, 653–668. https://doi.org/10.5194/tc-11-653-2017.

Xu, S., Das, S.K., Archer, L.A., 2013. The Li–CO 2 battery: a novel method for CO 2 capture and utilization. RSC Adv. 3, 6656–6660.

Yen, A.S., et al., 2005. An integrated view of the chemistry and mineralogy of martian soils. Nature 436 (7047), 49–54. https://doi.org/10.1038/nature03637.

Zacny, K., Bar-Cohen, Y., 2010. Drilling and excavation for construction and in situ resource utilization. In: Badescu (Ed.), Chapter 14 in Mars: Prospective Energy and Material Resources. Springer.

Zent, A.P., Hecht, M.H., Cobos, D.R., Wood, S.E., Hudson, T.L., Milkovich, S.M., DeFlores, L.P., Mellon, M.T., 2018. Initial results from the thermal and electrical conductivity probe (TECP) on Phoenix. J. Geophys. Res. Planets. https://doi.org/10.1029/2009JE003420@10.1002/(ISSN)2169-9100.PHOENIX2.

Zimmerman, W., et al., 2002. The Mars '07 north polar cap deep penetration cryo-scout mission. Aero. Conf. IEEE. https://doi.org/10.1109/AERO.2002.1036850.

Zuber, M.T., Phillips, R.J., Andrews-Hanna, J.C., Asmar, S.W., Konopliv, A.S., Lemoine, F.G., Plaut, J.J., Smith, D.E., Smrekar, S.E., 2007. Density of Mars' south polar layered deposits. Science 317 (5845), 1718–1719. https://doi.org/10.1126/science.1146995.